Politecnico di Torino

Master of Science in Petroleum and Mining Engineering
Academic Year 2022/2023

Master Thesis

BEST PRACTICES FOR PREPARATION OF SAMPLES FOR LABORATORY ANALYSIS

Supervisor:
Professor Francesca VERGA
Co-Supervisor:
Alessandro SURIANO

Candidate:
Christina ABOU MRAD

Abstract:

Core analysis is performed to measure the petrophysical properties of rock samples to be used in reservoir characterization, modeling, and performance predictions. In this study, the petrophysical properties, namely porosity and absolute permeability, of a set of eleven samples are measured through a well-defined methodology. First, the dimensions and dry weight of each sample are measured, then the porosity is estimated using two methods: through grain volume measurement, and through pore volume measurement. Then, the absolute permeability to gas is measured and corrected to liquid through the use of the Klinkenberg correlation. Eventually, each sample is saturated at atmospheric pressure, then dried and saturated again under pressure, all the while recording the saturation time for each step of the process. Using the wet weight at which the sample is fully saturated and the dry weight, a third porosity measurement method is performed. The time at which each sample reaches 100% water saturation is plotted against the petrophysical properties (porosity and permeability) of the same sample to assess any relationship between the time needed to reach 100% water saturation and the considered property. The results were that a correlation was possibly found between saturation time and absolute permeability. The relationship between saturation time and porosity was less evident. Furthermore, atmospheric pressure was not enough to fully saturate samples even when soaked for a relatively long time. Overall, this study provides suggestions on how to manage the saturation of a rock sample using water and investigates the possible issues that can be encountered while doing it.

Acknowledgements:

I would like to express my gratitude to the institution for welcoming me from my home university.

I would especially like to sincerely thank my supervisor Professor Francesca Verga for giving me the special opportunity to work in the Rocks and Fluids Laboratory to complete my master thesis.

I am also grateful to my co-supervisor Alessandro Suriano for guiding me and helping me in every step of this project.

Finally, I would like to convey my love and gratitude to my parents and brother for unconditionally supporting me to complete my studies.

Summary:

List of Figures:

List of Tables:

Chapter I: Introduction:

1.1. General Context:

1.1.1. Reservoir Characterization:

While seeking to correctly evaluate and develop recently located fields [1], it is crucial to ensure the collection of the most accurate set of information from a variety of disciplines [2] and use the obtained data to build a high-resolution model and get the clearest depiction obtainable of the subsurface of interest, the process of which is called reservoir characterization.

The main objective of reservoir characterization is to minimize technical and financial risks, maximize the economic value of the reservoir, and constantly evaluate the economic value of the reservoir throughout its life (Tiab and Donaldson, 2016) [1] as well as to predict the reservoir's performance. In order to achieve this goal, petrophysical, seismic, well log and production data are acquired.

Reservoir properties are obtained by combining petrophysical data with well logs, well tests

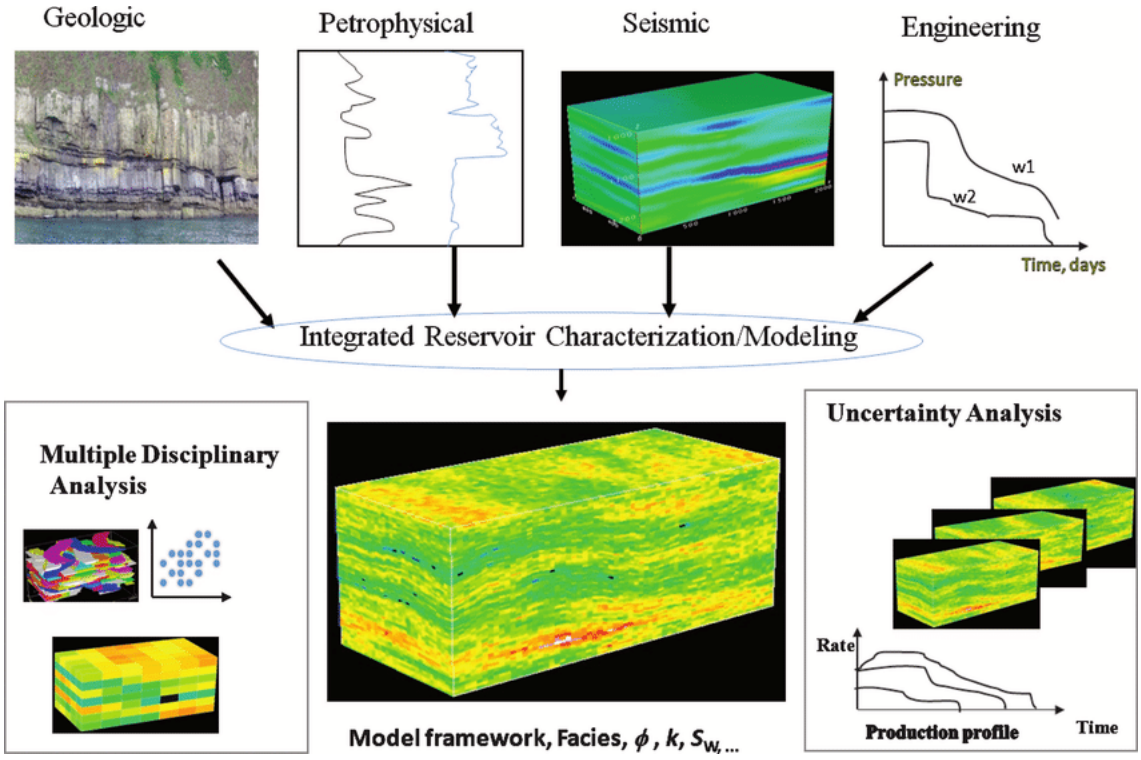

Figure 1: Reservoir Characterization and Modeling [3]

and core analysis. It is necessary to characterize the matrix properties of a reservoir and fluid distribution in the appraisal and development stages.

While well logs give highly reliable data on the position of the well, it is not enough to give information about its surroundings to cover the whole field since the number of wells is limited. [4] The same goes for core analysis, which is the most direct data yet only covers a small part of the well. [5] Meanwhile, seismic data holds a high level of uncertainty although it yields far larger coverage than well logs and core analyses. To solve this issue, geological and geophysical data are added to be able to extend the well information in order to fill the space of interest with a good properties' estimation.

Ultimately, with the acquired information, reservoir properties are estimated, and a model is built and calibrated as more information is obtained through core analysis and well logs.

1.1.2. Core Analysis

Core analysis is a direct method to measure reservoir properties through a series of laboratory tests performed on rock plugs sampled from cores, which are acquired by a coring process from the reservoir, well preserved and transferred to the laboratory. [6][7][8]

These rock properties obtained through core analysis are required in multiples stages of the

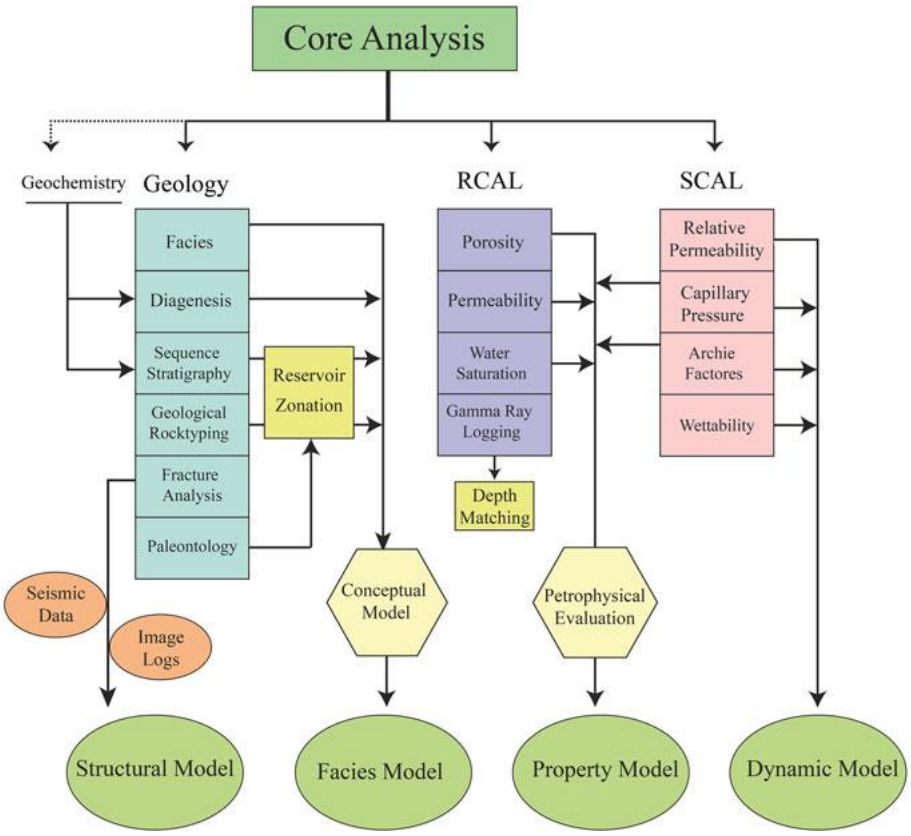

Figure 2: Core Analysis and End Goals [7]

entire life of a reservoir during the exploration phase in order to adjust well logs and seismic

data while choosing an optimal completion technique, in the development stage and during the production phase while estimating reserves and deciding on recovery methods. [6]

There are two main types of core analyses: Routine Core Analysis (RCAL) and Special Core Analysis (SCAL) [6][9]. During Routine, (or Conventional) Core Analysis, porosity, and absolute permeability of a dry, clean sample at ambient conditions as well as fluid saturations are measured in order to combine results with log data and to characterize reservoir properties. RCAL yields faster results and tends to be less expensive than SCAL. On the other hand, Special Core Analysis usually entails measurements of porosity at reservoir stress conditions, capillary pressure, relative permeability, resistivity index and formation resistivity factor, wettability, residual saturations, cation exchange capacity, NMR (Nuclear Magnetic Resonance) and CT (Computed Tomography), and other properties. [10][11][12][13][14][15][16][17][18]

In reservoir engineering, data obtained from RCAL and SCAL are indispensable as they affect the calculated potential amount of hydrocarbons, as well as the flow of each phase in the reservoir when appended to fluid properties.

1.2. Scope of the Study

Saturating rock samples with water or brine is a step often necessary before initiating laboratory analysis, Special Core Analysis (SCAL) in particular, namely relative permeability measurements. In this context, sample saturation was regarded as a preparatory step in a larger study [19][20]. As a consequence, there is little to no information in the literature about how to saturate samples, how long it might take, and if there is any relationship between the saturation process and the rock petrophysical properties, as well as indications on which other parameters might affect the process.

The objective of this study is to propose a sort of guideline for the saturation of rock samples with water in order to prepare them for Special Core Analysis and to highlight any relationship between the saturation process and the petrophysical properties of the rock samples subjected to it, such as porosity and permeability.

A methodology to follow will be detailed in this study where rock samples length and diameter are measured, afterward porosity and permeability are determined and finally, the sample is saturated in water. The parameters controlling the saturation process are constantly recorded. Ultimately, the results are interpreted to offer some insight into the saturation methodology and the expected time needed to complete the process.

Chapter II: State of the Art:

In this chapter, the parameters of interest to the study which comprise Porosity, Permeability and Saturation Time are introduced, and the methods of measurement are thoroughly described.

2.1. Porosity

According to Tarek Ahmed [21], the porosity of a rock is a measure of storage capacity (pore volume) that is capable of holding fluids. It is defined by the following equation:

$$\phi = \frac{pore\ volume}{bulk\ volume}$$

Equation 1

where ϕ is the rock porosity, pore volume V_p is the void space between the grains and bulk volume V_b is the total volume of the rock.

During the formation of rocks, some void spaces were isolated while others stayed interconnected. Thus, we can distinguish two types of porosity: absolute porosity and effective porosity.

Absolute porosity ϕ_{abs} includes all void spaces in the pore volume, both interconnected and isolated.

$$\phi_{abs} = \frac{V_p}{V_b} = \frac{V_b - V_g}{V_b} = \frac{V_p}{V_p + V_g}$$

Equation 2

On the other hand, effective porosity considers only interconnected pore volume with respect to the bulk volume. Effective porosity is of interest when calculating the recoverable amount of hydrocarbons or the volume of fluids that can be injected and stored in the reservoir.

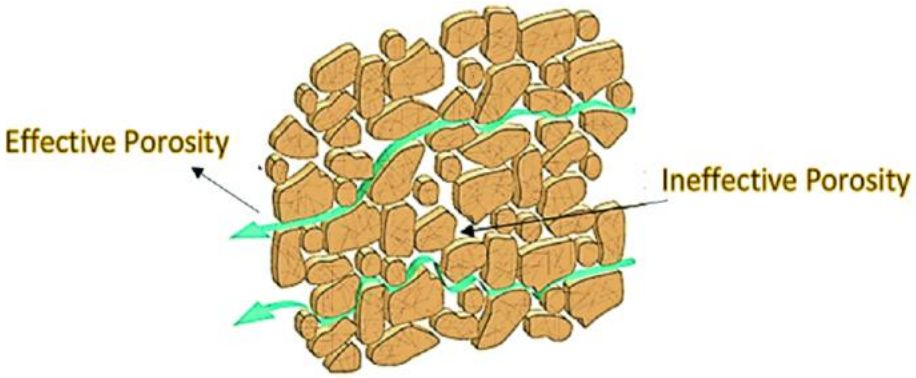

Figure 3: Illustration of Effective Porosity [22]

$$\phi_{eff} = \frac{V_{p,interconnected}}{V_b}$$

Equation 3

We also define original porosity which presented itself during sedimentation, and induced porosity which developed post-deposition due to a geological event, such as fracture development. [23]

Generally, a direct measurement of porosity is obtained through core analysis, which yields more accurate data when compared to well logs and seismic [6]. Although more accurate, core data covers a smaller portion of the reservoir than well logs. It is therefore good practice to compare core and log porosities at similar depths of the same well and calibrate the log data accordingly.

Porosity Measurement

Porosity is generally measured in the laboratory on cylindrical plugs, where two out of three volumes are determined: Grain Volume (Vg), Pore Volume (Vp) and Bulk Volume (Vb) to apply the absolute porosity equation (Equation 2).

There is a variety of methods to measure porosity which mainly differs between RCAL - which are cheaper and yield faster results - and SCAL - which are generally more expensive time-consuming but provide more accurate data and allow to replicate reservoir conditions. Generally, RCAL grain volume and pore volume at low confinement are measured using an inert gas; on the other hand, samples are saturated with brine to determine porosity in SCAL.

Before any RCAL, the samples must be well cleaned, dried and the dry weight must be recorded.

According to the literature, three main methods to measure porosity in RCAL exist:

a. Grain Volume Measurement:

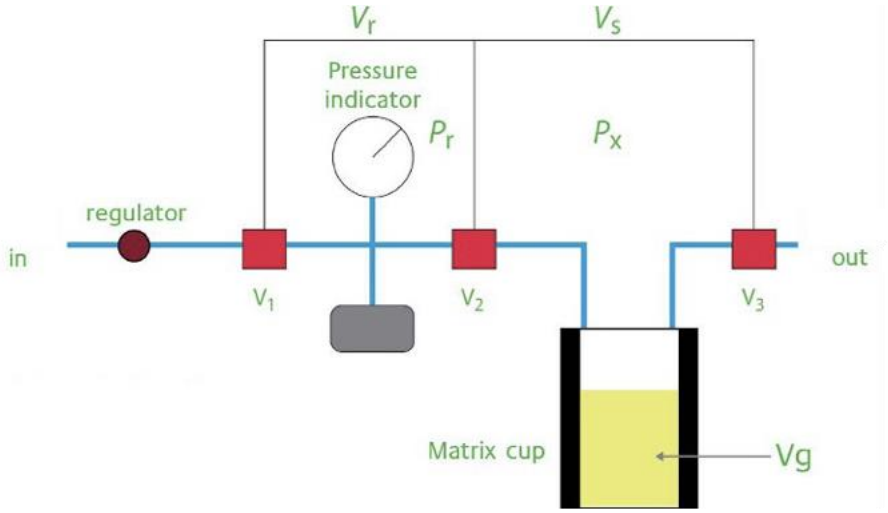

Figure 4: Grain Volume Measurement [9]

To obtain grain volume, the sample is inserted in a matrix cup connected to a gas tank with a valve in between. The valve V2 is initially closed, and the tank (gray box between V1 and V2 in Figure 4) is filled with an inert gas through valve V1 opening, letting pressure build up until a certain reference value, in this case study it is 100 psi. Then, valve V1 is closed and valve V2 is opened to let the gas expand into the matrix cup, filling all the void space. Pressure stabilizes and it is recorded. The calculation of the grain volume relies on Boyle's law which states that for an ideal gas, at a constant temperature,

$$P_{Ref}V_{Ref} = P_{Exp}V_{tot}$$

Equation 4

Where

P_{Ref}	Reference pressure before opening the valve
V_{Ref}	Reference volume which equates the volume of the gas tank
P_{Exp}	Expansion pressure recorded
V_{tot}	Total volume in which the gas expanded

The total volume in which the gas expands is none other than the volume of the gas tank plus the volume difference between the matrix cup and the grain volume of the sample. Knowing the value of all parameters except for one unknown, grain volume V_g can be calculated:

$$P_{Ref}V_{Ref} = P_{Exp}\left(V_{Ref} + V_{MC} - V_g\right)$$

Equation 5

$$V_g = \frac{P_{Exp}\left(V_{Ref} + V_{MC}\right) - P_{Ref}V_{Ref}}{P_{Exp}}$$

Equation 6

Where

V_g	Grain volume
V_{MC}	Volume of the matrix cup

This method is common in RCAL porosity measurements, it is fast, inexpensive, non-destructive, very accurate and repeatable as long as the equipment is calibrated. It is recommended to choose the larger sized sample having a diameter of at least 1.5 inches instead of the smaller, lower than 1 inch diameter, in order to minimize potential errors. It is also recommended to calibrate the equipment very often and to make sure that the temperature does not vary from the calibration temperature to reduce inaccuracies.

b. Pore Volume Measurement:

In this method, the shape of the sample must be as perfect as possible to yield accurate results. The system resembles the one used to determine the grain volume, but instead of using a matrix cup, the sample is placed in a core holder and is subject to a confining pressure to hold it with the help of a rubber sleeve, which may also

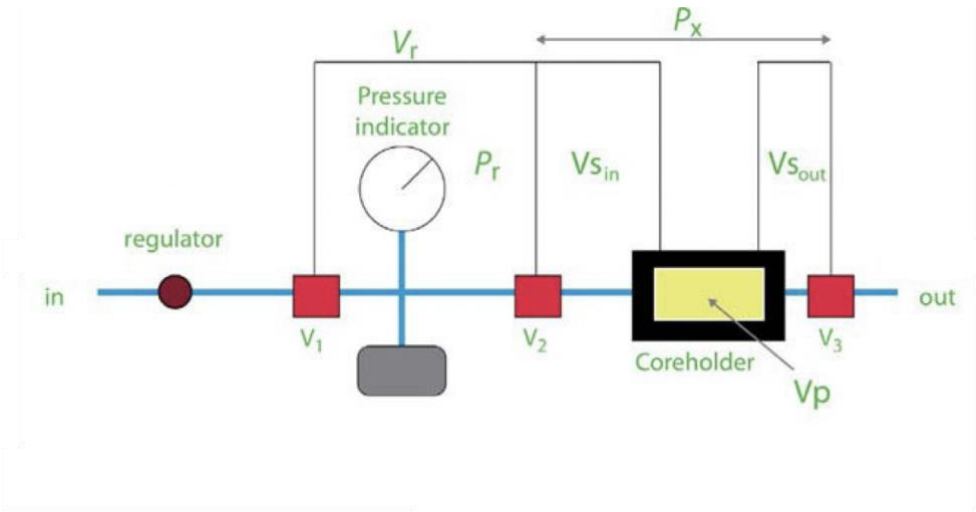

Figure 5: Pore Volume Measurement [9]

allow replicating reservoir stress conditions.

Boyle's law is applied in this method too, with the volume of pores being the only unknown. Since the sample is sealed, the reference pressure expands in the pore spaces of the sample, as well as the inlet and outlet platens of the core holder which are of known pore volume. The equation turns out to be:

$$P_{Ref}V_{Ref} = P_{Exp}(V_{Ref} + V_{in} + V_{out} + V_P)$$

Equation 7

And the pore volume is calculated:

$$V_P = \frac{P_{Ref}V_{Ref} - P_{Exp}(V_{Ref} + V_{in} + V_{out})}{P_{Exp}}$$

Equation 8

Calibration of the equipment is just as important for this method as for the previous one. This technique is highly recommended for unconsolidated samples [9]. It is fast in most cases, inexpensive, and non-destructive. Although, it is not convenient for irregularly shaped samples since this may produce inaccuracies.

c. Bulk volume measurement:

There are multiple ways to determine the bulk volume in Routine Core Analysis, one of them requires the use of a caliper and two of them involve mercury. The first method characterizes the bulk volume by measuring the dimensions of the sample using a caliper and calculating the volume of the cylinder. Although this method is

quite simple, it is not the most accurate considering that samples rarely have a perfect cylindrical shape.

More accurate methods to measure the bulk volume involve mercury, and two main tests can be performed. The first test is performed by using a mercury pycnometer, which is a pressure chamber in which the sample is inserted, and a mercury pump is connected to it, as well as a readout to determine the injected volume of mercury.

First, mercury is injected into the empty chamber until it reaches the top and the

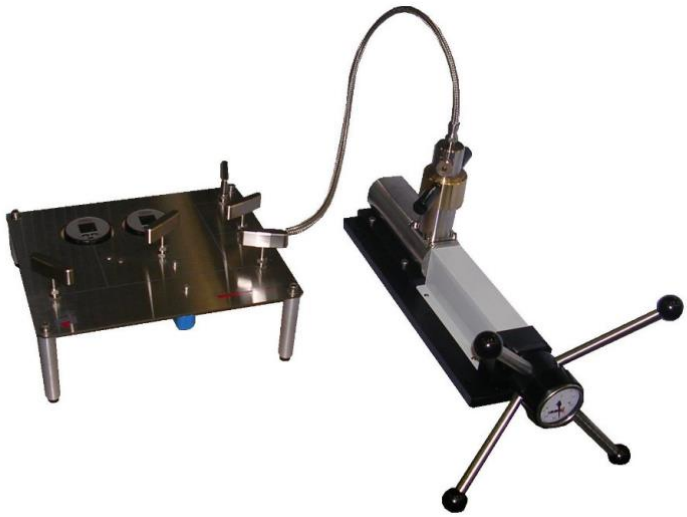

Figure 6: Mercury Pycnometer [9]

volume is recorded. The chamber is then emptied, and the sample is inserted. Then, mercury is injected again until it reaches the top. The bulk volume is finally calculated using the volume of mercury necessary to reach the same level obtained during the first injection.

The second test involves a mercury immersion system, where a mercury bath is placed on top of a balance. A cradle is lowered into the mercury to a reference mark, and the balance is tared. The cradle is withdrawn, and the sample is placed in the cradle, then re-immersed to the same reference mark. The increase in weight represents the immersed weight.

The bulk volume is then calculated as the ratio of the immersed weight over the

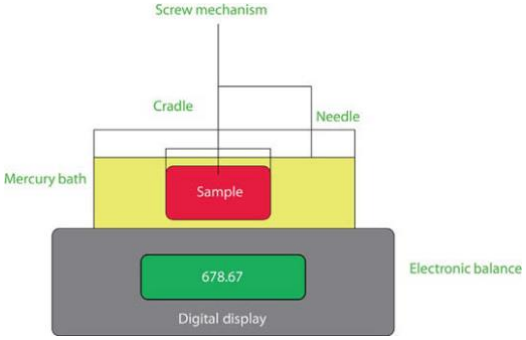

Figure 7: Mercury Immersion System [9]

density of mercury:

$$V_b = \frac{W_{imm}}{\rho_{Hg}}$$

Equation 9

Although the mercury tests give a more accurate measurement of the bulk volume, they are less used nowadays due to safety concerns around mercury vapors which prove to be toxic and so, safety protocols must be placed. Moreover, these methods are only accurate as long as mercury does not enter the pore spaces of the sample, otherwise the bulk volume would be underestimated and the sample would become invalid for further testing, as well as potentially toxic. It is not recommended to use mercury to test unconsolidated, fractured surface samples as well as samples with large pores surface.

d. Liquid saturation porosity measurement:

Since saturating a sample with formation water is usually the first step before a lot of SCAL laboratory tests, this method is seen as an additional opportunity to calculate the porosity of a sample saturated with a liquid of known density. A comparison with the porosity obtained from the previous methods can be made. First, the sample is cleaned, well dried and the dry weight is measured on a precision balance. Then, it is placed in a saturator and is saturated in deaired saturating fluid, generally Synthetic Formation Water SFW. How the saturator works is then deeply explained in Chapter III. In the case of low permeability samples, it is pressurized and left for a couple of days to make sure that the pores are fully saturated. Finally, the weight of the fully saturated sample is measured. [9][48]
In this test, the pore volume is determined by subtracting the weight of the saturated sample from its dry weight and then dividing the difference by the saturating fluid's density which is known.

$$V_{p_{sat}} = \frac{W_{sat} - W_{dry}}{\rho_{fluid}}$$

Equation 10

Where

$V_{p_{sat}}$	Pore volume obtained from liquid saturation
W_{sat}	Weight of saturated sample
W_{dry}	Weight of dry sample
ρ_{fluid}	Density of the saturating fluid

While the measurement of weights makes this method more accurate than the previous one, it is more costly and takes more time to perform. Moreover, if it shows to be lower or higher when compared to previously measured data, it could mean that the pores were not fully saturated (lower), or that the samples were subject to grain

loss (higher). This phenomenon was observed by Ji-Quan Shi et al. who saturated sandstones and performed a CT scan before initiating their experiment. The CT saturation data revealed that the sample was not fully saturated, with a 4.2% residual air saturation for the first type of sandstone, and a 3.5% saturation for the second type, which they attributed to unconnected pores unreachable to the saturating fluid [24][25].

2.2. Permeability

The permeability is a property intrinsic to the reservoir formation which dictates the capability of fluids to flow through a porous medium. [9][26] Three types of permeabilities are distinguished:

Absolute Permeability (k) which is measured when only one phase completely fills the pore space, Effective Permeability (k_{eff}) which is the permeability measured for one fluid phase when multiple fluids are present, and Relative Permeability (k_r) which measures the effective permeability to one phase with respect to the absolute one.

The property is defined quantitatively through Darcy's law for fluid flow expressed below:

$$v = \frac{q}{A} = -\frac{k}{\mu}\frac{dp}{dl}$$

Equation 11

Where,

v	Apparent velocity
q	Flow rate
A	Cross-sectional area
k	Absolute Permeability
μ	Viscosity
$\frac{dp}{dl}$	Pressure gradient

Through some quick mathematical development and integration, we can extract the equation for permeability:

$$k = \frac{q\mu L}{(P_1 - P_2)A}$$

Equation 12

Where

L	Length of the sample
P_1	Inlet pressure
P_2	Outlet pressure

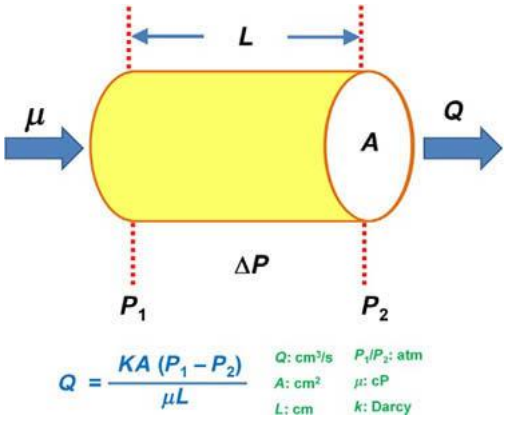

Figure 8: Representation of Darcy's Law [9]

Although Darcy's law is widely used in petroleum engineering, it is subject to the assumptions that the flow is horizontal, rectilinear, steady-state conditions are applied and the fluid is incompressible. If these conditions could be considered true for liquids, they do not apply to compressible gases. [27]

Thus, Darcy's law was corrected to account for gases. [9][21] The gas is assumed to act like an ideal gas at low pressures, and therefore,

$$P_m Q_m = Q_{atm} P_{atm}$$

Equation 13

Where,

P_m	Mean pressure
Q_m	Mean gas flow rate
Q_{atm}	Flow rate at atmospheric conditions
P_{atm}	Atmospheric pressure

With

$$P_m = \frac{P_1 + P_2}{2}$$

Equation 14

And the equation for the permeability to gases becomes:

$$k_g = \frac{Q_{atm} P_{atm} \mu L}{P_m (P_1 - P_2) A}$$

Equation 15

$$k_g = \frac{2 Q_{atm} P_{atm} \mu L}{(P_1 + P_2)(P_1 - P_2) A}$$

Equation 16

$$k_g = \frac{2Q_{atm}P_{atm}\mu L}{A(P_1^2 - P_2^2)}$$

Equation 17

This Darcy equation for permeability to gas now considers the compressibility of gases. It is visible when comparing it to the equation for liquids that the former has a pressure difference in the denominator, and that the flow is considered constant. Meanwhile, in the equation for gases, the difference in the denominator is of squared pressures, and that the flow rate is no longer considered constant at the inlet and the outlet, instead, the flow rate in the equation is now the outlet flow rate which is assumed to be at atmospheric conditions.

2.2.1. Absolute permeability measurement:

Absolute permeability is generally measured in Routine Core Analysis by flowing air or nitrogen through a dry, clean sample at ambient conditions; contrarily, in Special Core Analysis, the measurements can be developed under conditions (temperature, pressure, type of fluids…) that are more representative of a reservoir. In RCAL, there are some assumptions which can be considered valid for nitrogen, such as taking the compressibility factor as unity and assuming the gas temperature equal to its temperature at atmospheric conditions. Moreover, other assumptions are set for Darcy's law to keep it valid: the fluid must be inert, the flow must be laminar, and a single phase must be considered, and permeability must be assumed constant through the sample domain and must not be rate dependent. If the first and third conditions are true for nitrogen, the other conditions do not necessarily apply due to the flowing fluid being a gas, which means that the permeability is not constant due to

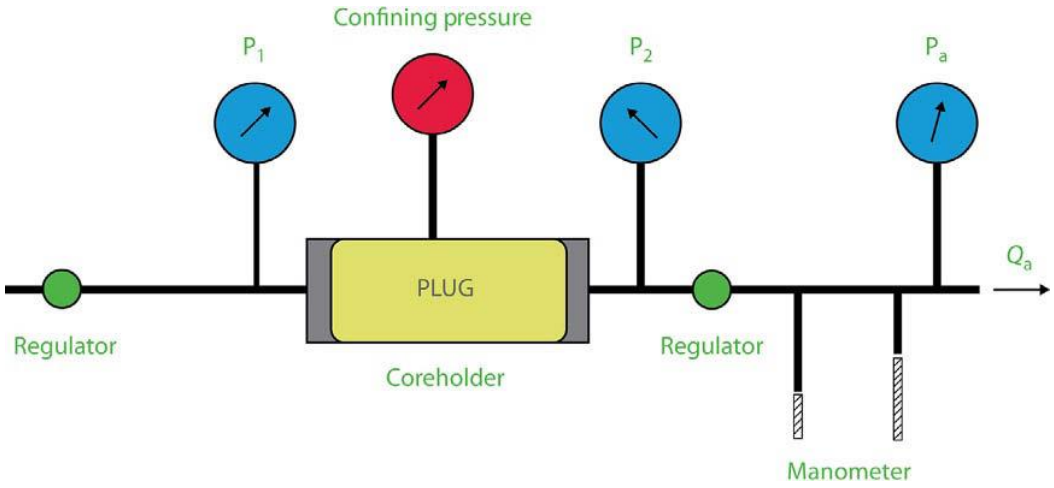

Figure 9: Absolute Permeability Measurement [9]

Klinkenberg effects, and the flow may not be laminar if certain rates are imposed. [23]

To run a permeability measurement, the sample is inserted into a core holder lined with a rubber sleeve to confine it. The sample must be sealed in order to avoid any gas from bypassing the sample. Pressure transducers are placed at the inlet and at the outlet of the sample. A gas regulator is set to control the inlet pressure, a back pressure regulator is generally set to control the outlet pressure and a flow of nitrogen is conveyed through the

sample at a constant rate. As the pressure stabilizes, all the parameters necessary to calculate the permeability are recorded. [9]

2.2.2. Klinkenberg effect:

Until a certain point, the permeability was considered to be intrinsic to the porous medium and independent from the fluid used to measure it, yet a large discrepancy was found between air and water permeabilities with the second having a lower value than the first [28]. This difference was particularly prominent in low permeability samples [28]. To further investigate this phenomenon, permeability measurements were done on a variety of liquids, and found that they yielded comparable results within the margins of error. On the other hand, when measurements were performed using different gases, different values of permeability were obtained. It was deduced that the discrepancies were due to the behavior of gases. The theory of slip was introduced which states that during gas flow, the gas near the walls has a finite velocity with respect to the solid wall; moreover, at the walls, the velocity gradient is higher than when it is farther from the wall [28]. The slip effect was applied to capillaries in which gas flow is present, and equations were developed and combined with Darcy's law for gas flow in a porous medium, to finally obtain a relationship between the apparent permeability and the actual permeability of a porous medium:

$$K_a = K\left(1 + \frac{b}{P_{mean}}\right)$$

Equation 18

Where

K_a	Apparent permeability
K	Klinkenberg permeability
b	Constant, gas slippage effect
P_{mean}	Mean pressure

The apparent permeability is the permeability to gas, and according to the equation above it has a linear relationship with the inverse of the mean pressure. The intercept of this linear function is extrapolated to yield the Klinkenberg permeability. The Klinkenberg permeability was compared to the permeability to liquid and similar values were found within error [28].

2.2.3. Limitations to permeability measurement:

It is important to keep in mind that the permeability measurements run with gases are subject to conditions on the flow regime, mainly that the flow needs to be laminar in order to be able to apply Darcy's law. If the flow rate is too high [9], the flow regime becomes turbulent, and an additional pressure drop is created. Regarding the instrument used in this study to measure permeability, the flow rate is controlled by the applied pressure gradient which must not exceed around 4 psi/inch for low permeability samples, and around 0.5 to 1.2 psi/inch for high permeability samples. If these indicative values are surpassed, Darcy's law is no longer applicable, and if the condition is not respected, the experiment would result in an underestimation of the permeability value.

2.3. Saturation of Water:

Fluid saturation is the volume of a fluid that occupies the pore volume. It is expressed as a fraction or as a percentage, and ranges from 0% where there is no fluid in the pore space to 100% where all the pore space is filled with fluid. The equation is as follows:

$$S_{fluid} = \frac{volume\ of\ fluid}{volume\ of\ pores}$$

Equation 19

In the presence of multiple fluid phases, the sum of all saturations in a fully saturated sample should be equal to 100%.

In this study, the main interest is on water saturation, therefore, the equation becomes:

$$S_w = \frac{volume\ of\ water}{pore\ volume}$$

Equation 20

Saturating samples:

The saturation process is performed using a manual saturator. How the saturator works is explained in Chapter III.

Although not much information is present in the literature about the process, saturating rock samples is generally the first step prior to a number of tests performed in Special Core Analysis. One application of the saturation process is to prepare samples for the determination of capillary pressure curves through a series of imbibition and drainage displacement processes, where imbibition is the process of a wetting fluid displacing a non-wetting fluid, and drainage is when a non-wetting fluid displaces a wetting fluid [29][30]. Another instance where saturation is performed was an experiment where samples were saturated before being subjected to a gas-driven drainage process to determine gas relative-permeability curves. [31]

Some equipment that is used in laboratories comprises CT scanning to determine the saturation or to monitor the saturation variations while performing tests such as water flooding, or CO_2 flooding of saturated cores. NMR may also be used to obtain information on liquid saturations. [24][25][14][32]

Chapter III: Materials and Methods:

In order to fulfill the requirements of this study, a series of laboratory tests were conducted on a set of rock samples to measure the parameters needed, which are porosity, permeability, and the time needed to saturate the samples. In this chapter, the equipment used to obtain experimental data is introduced, as well as the methodology to be followed while performing the tests.

3.1. Equipment

To be able to perform laboratory tests it is important to have at hand all the equipment needed, and to understand how each of the machinery works.

3.1.1. PoroPerm:

PoroPerm is used to obtain values of porosity and permeability for an appropriately sized rock sample. This machine measures the rock porosity using two different methods: either by estimating grain volume using a matrix cup, or by estimating pore volume using a core-holder. Permeability measurements may also be performed in the same core-holder by switching the dial to Permeability Mode. The measurement methods for Vg, Vp and permeability are described in the previous chapter (refer to Chapter II). The fluid used to run these measurements in the laboratory is nitrogen.

Figure 10: PoroPerm Equipment

3.1.2. Manual Saturator:

The manual saturator is used for more than one purpose. Before using this equipment, however, it is of critical importance to measure the dry weight of the sample with a precision balance. To use the saturator, the sample is inserted into a tank with billets to reduce the dead volume as much as possible, they help to speed up the process. The water container attached

to the machine is filled and a vacuum pump is connected. For this kind of experiment, tap water was used. Using brine would have been much more representative of reservoir fluid but, due to technical issues (salts could deposit clogging part of the system such as its check valves) it was impossible. The role of the vacuum pump is to remove air particles present both inside the sample pore spaces and in the water that will saturate them. The pump is turned on and left for a while until significant ebullition is no longer present which means that all air is removed from the chamber and that the water is fully de-aerated. The pump is then switched off and disconnected from the apparatus, which will cause the water to enter the vacuumed chamber containing the rock sample. The valve connecting the system to the environment is closed – therefore the system is now closed – and a hand pump is used to pressurize the tank to a value of choice. Once pressurized, the duration of which the sample is kept under pressure is recorded. The valve is then opened to stop the process. The sample is carefully extracted, and its wet weight is measured using the precision balance.

Figure 11: Manual Saturator

Common laboratory equipment such as a Vernier caliper and a precision balance were used as well.

3.2. Methodology:

To ensure that the most accurate measurements are obtained in the most efficient way, the following steps are followed for each rock sample:

I. *Sample dimensions:*
The length and diameter of the sample are measured with a caliper.

II. *Dry weight:*
The dry weight of the sample is recorded using a precision balance.

III. *Grain volume:*
The sample is inserted in the matrix cup of PoroPerm to measure grain volume and estimate porosity using the first method. Porosity measurements are run three times

for redundancy, afterwards, the porosity value is taken as the average of the three values obtained.

IV. *Pore volume:*
The sample is placed in the core-holder of PoroPerm to measure pore volume and obtain a second estimate of porosity. Measurements are run three times in this case as well and the average value between all three is taken.

V. *Permeability:*
Permeability to nitrogen is measured in the core-holder five times while varying the inlet and the back-pressure in order to plot the permeability to gas versus the inverse of the sample mean pressure and Klinkenberg permeability is then estimated.

VI. *Dry weight:*
The dry weight of the sample is measured again to account for any changes such as grain loss that could occur during previous tests. It is worth noting that in this study, no significant variation in dry weight was observed at this stage.

VII. *Saturation process:*
The sample is placed in the manual saturator to start the saturation process. The saturation time and pressure are recorded.

VIII. *Wet weight:*
The sample is removed from the saturator and is rolled on a damp cloth prior to weighing in order to remove excessive water at the surface of the sample and avoid any weight oscillation over 0.01 grams. The cloth is damp in order to avoid accidental variations of water saturation due to a capillary action if the saturated sample is put in contact with a dry fabric. The sample's wet weight is then recorded.
Swift weight measurement is crucial in this step because if the sample is left exposed for too long on the balance, the weight may decrease due to water evaporation.

The last two steps are repeated until a constant wet weight for the sample is obtained.

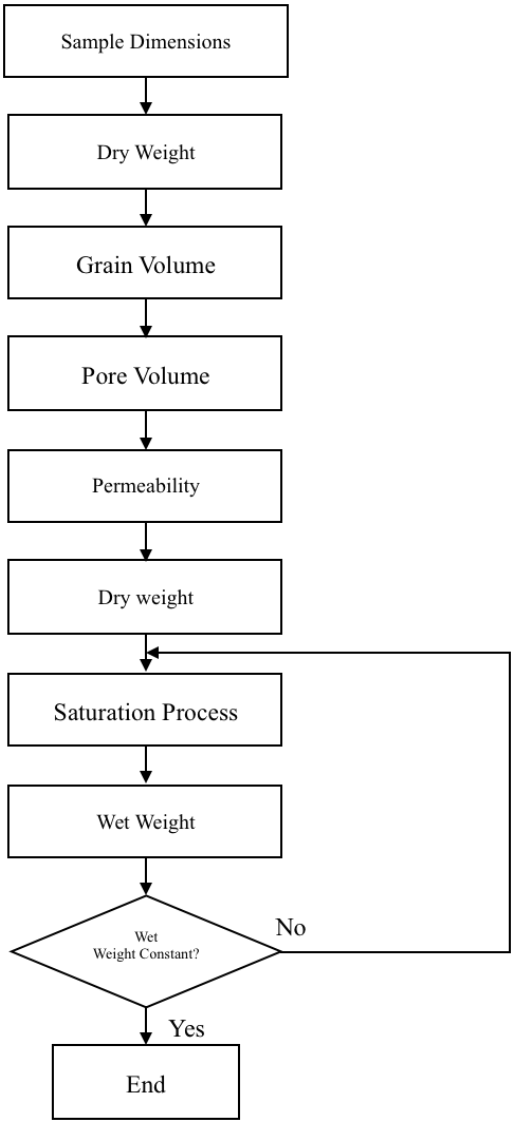

Figure 12: Algorithm of the Methodology

In this study, samples of four rock types will be tested: coarse sandstones, medium-to-fine sandstones, carbonates and calcarenites. Coarse sandstones are expected to yield very high porosity and very high permeability values. They are also expected to saturate rather quickly. Medium-to-fine sandstones are expected to have high porosity but a lower permeability. Carbonates usually have high porosity and low permeability, and calcarenites commonly have low porosity and low permeability, and they are expected to be the slowest to saturate.[33][34] [35] [37]

Some potential issues to expect during experimentation would be the immediate saturation of the coarse sandstones and so the failure to capture the correct time needed to reach 100% water saturation as well as the evolution of the water saturation with time. Moreover, potential sediment deposition could occur for sandstones and calcarenites, but it is not expected to be a significant problem for carbonates.

Chapter IV: Experimentation:

In this chapter, experiments conducted in the laboratory while following the steps mentioned in the previous section will be described, beginning with how the plugs are prepared, followed by the porosity and permeability measurements, as well as any problems faced during the tests. Finally, the sample saturation experiments carried out at different pressures are detailed.

4.1. Sample preparation:

The samples were cut into cylinders of 1.5-inch diameter and up to three inches in length, cleaned and dried. Then, the diameter and length of each sample were measured, and the dry weight was recorded. The rock type, dry weights, as well as the dimensions of each sample are resumed in Table 1.

Figure 13: Samples (from Left to Right, Top: CLC2, CLC3, MFS2; Medium: CLC1, CRB2; Bottom: CRB1, MFS1, CRB3)

Table 1: Sample Dimensions, Rock Type and Dry Weight

Sample ID	*Diameter (mm)*	*Length (mm)*	*Rock Type*	*Dry Weight (g)*
CS1	37.5	74.8	Coarse sandstone	155.05
CS2	37.2	75.6	Coarse sandstone	155.33
CS3	37.1	75.1	Coarse sandstone	151.54
MFS1	37.6	72.3	Medium-to-Fine sandstone	173.99
MFS2	38	73.9	Medium-to-Fine sandstone	176.88
CRB1	37.9	69.3	Carbonate	162.95
CRB2	37.5	72.4	Carbonate	180.83
CRB3	37.4	72.16	Carbonate	210.28
CLC1	37.4	72.4	Calcarenite	190.67
CLC2	37.1	73.7	Calcarenite	199.03
CLC3	37.4	74.9	Calcarenite	201.67

4.2. Porosity and Permeability Measurements:

The porosity measurements performed using the Matrix Cup were seamlessly collected for all samples. The porosity measured using the Core Holder was collected for most of the samples as well. The permeability to gas was run multiple times at different inlet pressures and back-pressures and plotted to obtain the Klinkenberg permeability for each sample. The reason why measurements were not performed on all the available samples was due to the failure of the core-holder prior to experiment completion. Furthermore, some problems were faced while running the tests on low permeability samples. Not only were the tests taking significantly more time than they did for the rest of the samples, but they were not always successful. In fact, for low permeability samples, the tests had to be run at very small flow rates, sometimes as low as the machine's lowest measurable flow of 0.5 milliliters per minute in order to stay within Darcy conditions and the pressure would still not stabilize enough for the software to estimate a value of gas permeability. This issue led to difficulties in obtaining five measurements of gas permeability to plot and obtain the Klinkenberg permeability which was the case for sample CLC2 where permeability was obtained using only three measurements. Moreover, the accuracy of the permeability values obtained for samples CLC2 and CLC3 is questionable, since the pressure drop is quite close to the limit value which, if surpassed, would lead to non-Darcy behavior and ultimately unreliable measurements.
The collected data are reported in Table 2.

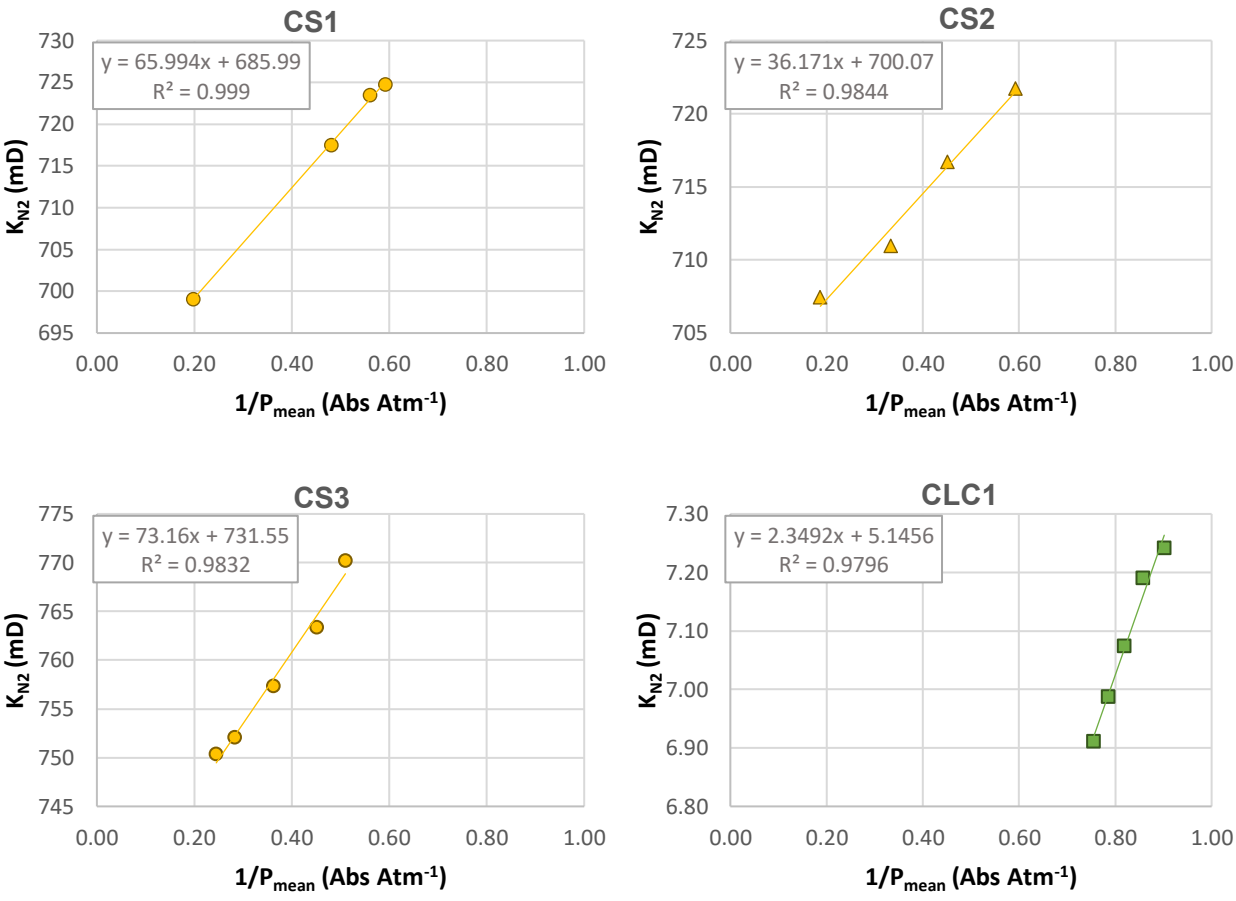

Figure 14: Klinkenberg Permeability Determination (Part 1)

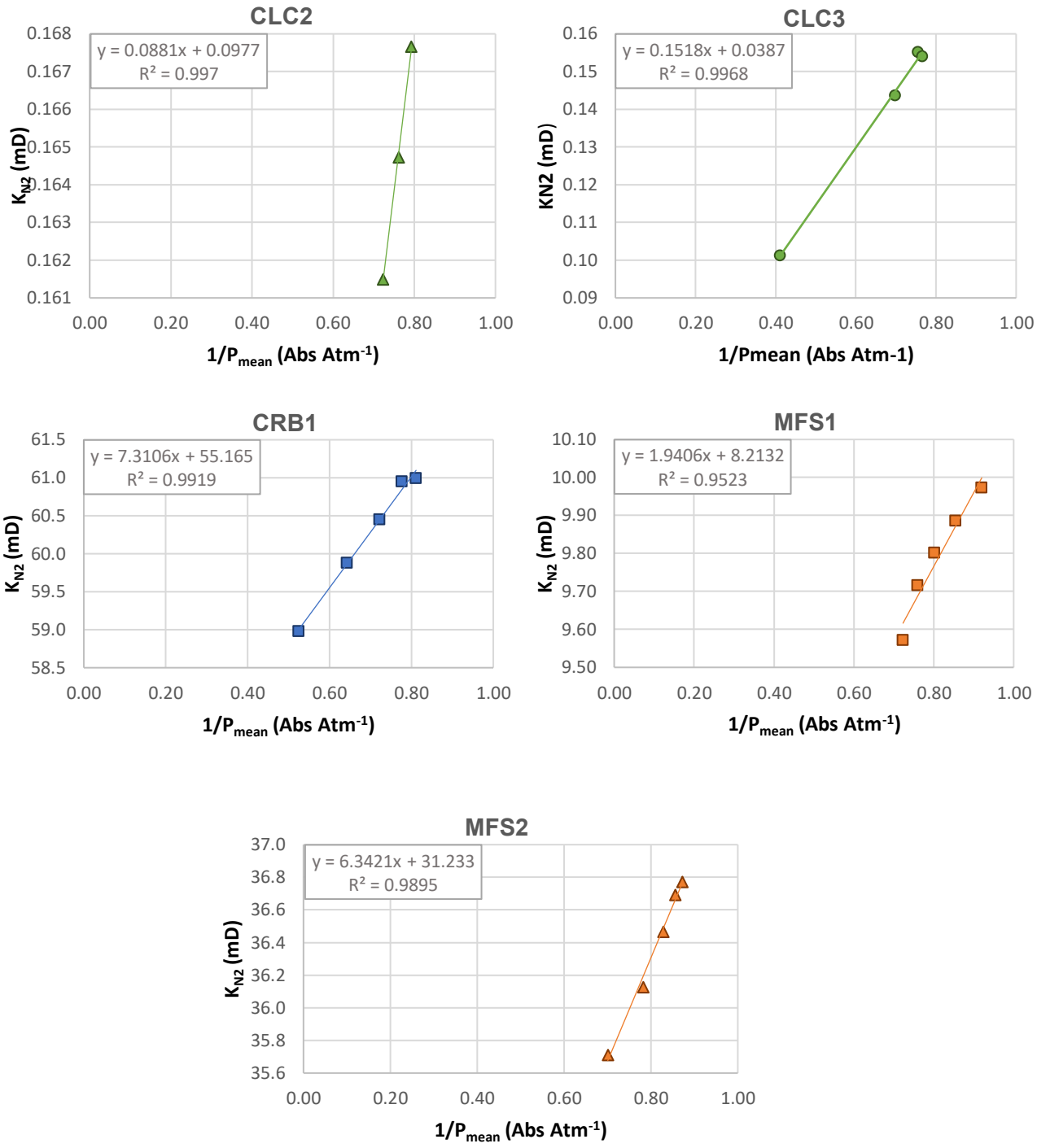

Figure 15: Klinkenberg Permeability Determination (Part 2)

Table 2: Samples Porosity from Grain Volume (GV) and Pore Volume (PV) Measurements and Klinkenberg Permeability

Sample ID	*Porosity GV*	*Porosity PV*	*Permeability k_L (mD)*	R^2
CS1	28.50%	24.77%	686	0.999
CS2	28.58%	24.49%	700	0.984
CS3	29.13%	24.40%	732	0.983
CLC1	13.75%	11.15%	5.15	0.977
CLC2	6.94%	6.80%	0.0977	0.997
CLC3	9.21%	7.58%	0.0387	0.997
CRB1	21.45%	20.85%	55.2	0.992
CRB2	15.86%	N/A	N/A	N/A
CRB3	1.44%	N/A	N/A	N/A
MFS1	17.92%	N/A	8.21	0.952
MFS2	19.65%	19.31%	31.2	0.989

4.3. Saturation time measurement:

To be able to ultimately compare results for different scenarios, the water saturation as a function of time was initially measured at atmospheric pressure for a variety of samples, then the samples were dried and saturated again at higher pressures.

4.3.1. Saturation at atmospheric pressure:

In this case, the dry weight of the sample was measured with a precision balance before saturation. A container was then filled with water and the plug was submerged while counting the time [34] as shown in Figure 15. After that, the sample was taken out and the wet weight was measured, then the sample was submerged again.
The process was repeated with thirty second time steps at first. Later on, the intervals were increased when it became noticeable that the wet weight was not increasing as much anymore for each step.

Figure 16: Saturation at Atmospheric Pressure

The data for the first few hours of saturation at atmospheric pressure are presented in Table 3 and plotted in Figure 17, where the evolution of water saturation with time can be appreciated. Saturation was calculated based on the porosity measured using the Pore Volume method.
It is quite clear from the plot that higher permeability samples, such as the three coarse sandstones, reached a high saturation within a short time, while lower permeability samples were remarkably slower to saturate.
Although the water seemed to penetrate the sample quite quickly at first, its infiltration slowed down to the point at which the wet weight of the plugs minimally increased, even when left immersed for nearly 2 weeks.

In fact, it is noticeable in Figure 18 that the water saturation never reached a value above 88%, not even for the most permeable of the tested samples. This phenomenon could be attributed to the instantaneous imbibition limiting values of a water-wet system, where water spontaneously infiltrates the sample while displacing another fluid until a certain limit where pressure must be applied to let more water penetrate the rock. [30][36][39][40]
The experiments performed to measure the time needed to reach 100% water saturation at atmospheric pressure ceased when it became clear that it would be quite difficult to obtain fully saturated samples in a reasonable time frame, which was impractical for the purposes of this study.

Table 3: Sample Water Saturation at Atmospheric Pressure and Wet Weight at each Time Step

Sample ID	Time (s)	Wet weight (g)	Sw (-)
CS1	1	161.97	0.331
	30	165.11	0.483
	60	166.57	0.554
	90	167.78	0.613
	120	168.79	0.662
	240	169.81	0.711
	360	170.2	0.73
	660	170.22	0.731
	1980	170.14	0.729
	5580	170.12	0.727
	9180	170.86	0.726
	86400	172.36	0.762
	360840	173.6	0.834
CS2	30	165.61	0.500
	60	166.91	0.564
	90	167.35	0.586
	120	167.93	0.615
	240	168.53	0.644
	360	169.04	0.669
	660	169.4	0.687
	1860	169.42	0.688

	9060	169.44	0.689
	86400	170.25	0.729
	1029600	172.91	0.860
CS3	1	156.67	0.265
	30	159.26	0.395
	60	160.02	0.433
	90	160.75	0.469
	120	161.28	0.496
	240	162.97	0.581
	360	164.04	0.634
	660	165.02	0.683
	1860	165.28	0.6962
	5460	165.27	0.6959
	9060	165.53	0.709
	19860	165.67	0.716
	943200	169.02	0.883
CLC1	30	192.37	0.193
	60	192.8	0.241
	90	193.04	0.268
	120	193.17	0.283
	240	193.59	0.329
	360	193.82	0.355
	660	194.33	0.412
	1860	195.51	0.544
	9060	196.09	0.609
	86400	196.46	0.65
	932400	198.1	0.834
CRB1	1	165.46	0.161
	30	167.35	0.275
	60	168.28	0.332
	90	168.84	0.366
	120	169.32	0.396
	240	170.26	0.453
	360	170.95	0.495
	660	171.91	0.553
	1980	172.57	0.593
	5580	172.58	0.594
	9180	172.53	0.591
	1032420	175.19	0.753
MFS2	1	176.96	0.0149
	30	177.12	0.0244
	60	177.22	0.0308
	90	177.25	0.0327
	120	177.31	0.0361
	240	177.36	0.0396
	360	177.45	0.0447

	660	177.54	0.0503
	1980	177.81	0.0673
	5580	178.25	0.0939
	9180	178.61	0.116
	1031100	190.21	0.827

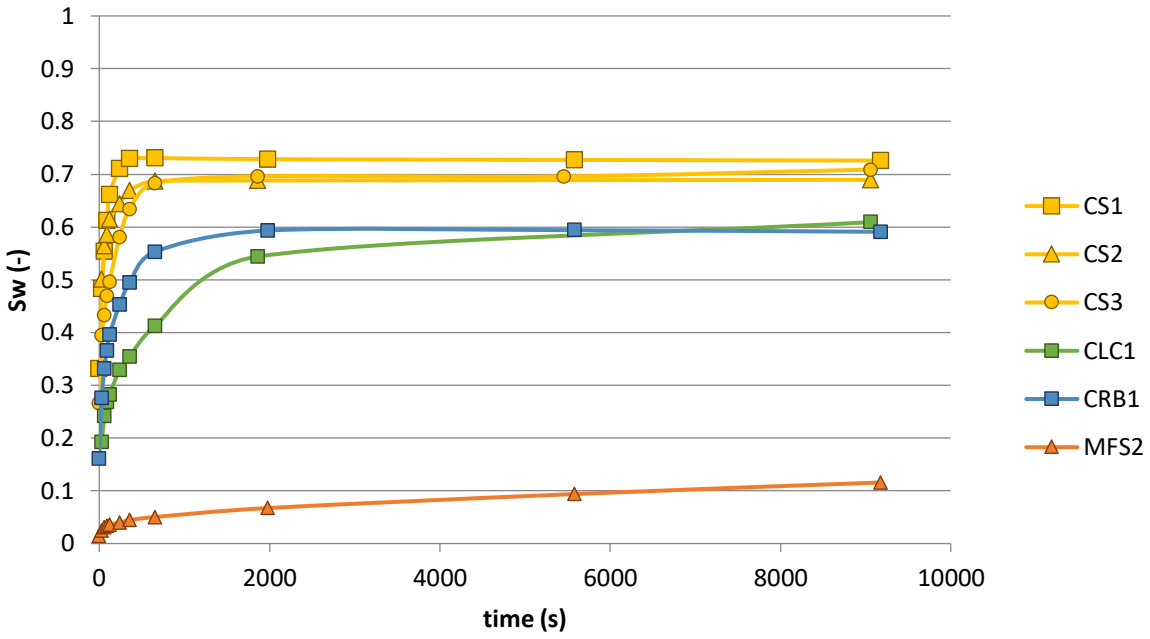

Figure 17: Evolution of Water Saturation at Atmospheric Pressure (short-term)

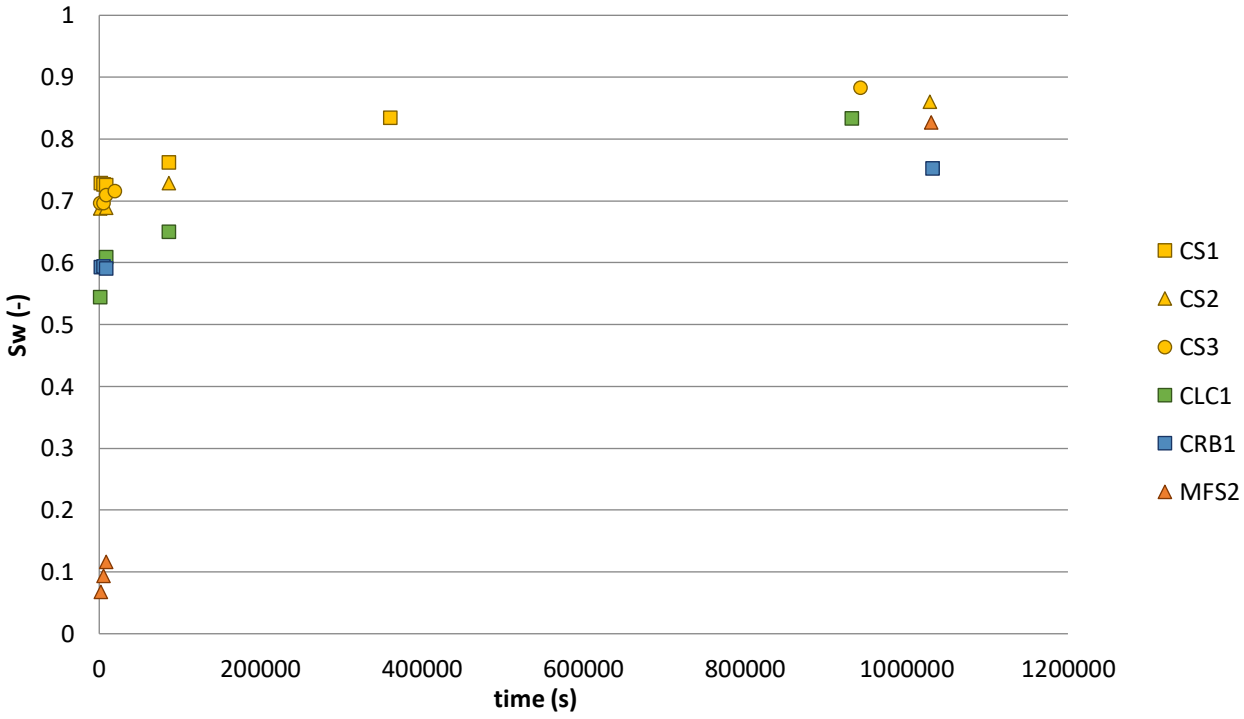

Figure 18: Evolution of Water Saturation at Atmospheric Pressure (long-term)

4.3.2. Drying samples:

To be able to repeat the experiments, the samples are placed in an oven with forced ventilation to dry for at least five hours and 60°C. Some samples did not reach their original dry weight, for them the drying process was repeated on the following day. The times and temperatures needed to dry each sample are reported in table 4. These times and temperatures must be considered indicative since there is no hint that they represent the ideal conditions to dry the samples. The drying process was interrupted at the moment that the weight was found similar to the initial one (Table 4, reported also in Table 5), but the weight of the sample was measured only a few times and with no consistency in the time steps since drying process was not the purpose of this study. It is worth mentioning that when left overnight, the weight of some samples slightly increased (Table 5) which may be due to ambient humidity adsorption. [41][42] The weight variation overnight was around $\pm 0.2\%$ where Coarse Sandstones, Calcarenites and most Carbonates showed an increase in weight, while CRB3 and MFS1 were subject to a slight decrease in weight. This weight variation could be considered insignificant enough that it will not affect results. The sample CS3 presented a dry weight that is slightly lower than its initial weight. The reason for this is that the sample was used for a relative permeability test out of the scope of this thesis between the saturation process at atmospheric pressure and the saturation process at 800 psi and it suffered grain loss in this test.

Table 4: Drying process applied to each sample

Sample ID	*Initial Weight (g)*	*Dry Weight (g)*	*Temperature (°C)*	*Time (h)*
CS1	155.46	155.05	60	10
CS2	155.42	155.33	60	10
CS3	151.99	151.54	60	10
CLC1	190.65	190.67	70	11
CLC2	199.06	199.03	70	6.5
CLC3	201.66	201.68	70	6.5
CRB1	162.87	162.95	60	10
CRB2	180.82	180.83	70	6.5
CRB3	210.17	210.28	70	11
MFS1	173.96	173.99	70	6.5
MFS2	176.72	176.88	60	10

Table 5: Samples Weights Before and After Each Drying Process

Sample ID	*Weight before drying (g)*	*Weight after 6.5h in oven at 70°C (g)*	*Weight when left overnight (g)*	*Weight after other 6.5h in oven at 70°C (g)*
CS1	176.32	154.39	154.71	154.37
CS2	176.35	154.92	155.26	154.9
CS3	168.87	148.08	148.38	148.01

CLC1	201.25	190.48	190.68	190.48
CLC2	207.62	199.78	199.85	198.0
CLC3	211.53	201.01	201.85	199.85
CRB1	178.97	162.64	162.95	162.61
CRB2	193.3	180.74	180.77	180.72
CRB3	211.62	210.63	210.42	210.30
MFS1	187.63	174.08	173.97	173.78
MFS2	192.38	176.88	176.89	176.31

4.3.3. Saturation under pressure:

4.3.3.1. Saturation at 800 psi:

Since the saturation of the plugs at atmospheric pressure failed to yield fully saturated samples, the time needed to obtain a complete water saturation could not be recorded. After the drying process, the experiments were carried out once again using a manual saturator allowing it to reach a higher pressure. The workflow of the manual saturator is duly described in Chapter III.

Since the process is completely analog, the values of pressure and time are quite difficult to assess with extreme accuracy. Not so accurate time steps and pressures are due to human imprecision. Each sample was saturated at a pressure close to 800 psi for time steps changing from a few to dozens of seconds depending on the sample's rock type.

While using the hand pump of the saturator to pressurize the vessel, it was noticeable that the pressure was decreasing slightly. This is perhaps due to the water filling the pore space and contributing to the pressure oscillation.

The sample was then removed from the chamber, weighed, and inserted again to saturate. The sample is assumed to be fully saturated when its wet weight remains constant between two consecutive steps, although it is not necessarily true. It is probable that a small fraction of air remains in the plug after saturation, [32] estimated to be around 3.5% to 4%. [24][25] As the weight becomes constant and neglecting this issue, the porosity can be calculated using Equation 10.

It is important to note that, for the purpose of this study, the weight is considered constant when it does not increase by more than 0.01 grams between two consecutive steps. Moreover, the sample is considered fully saturated if a decrease in weight is observed between the two steps.

Now that the porosity is obtained, the water saturation can be calculated for each time step. One issue remains before being able to plot the evolution of water saturation with time, which is that during the last time step, at any moment, the sample could have been fully saturated and not necessarily at the time the sample was extracted from the chamber. Thus, to solve this problem, each sample's saturation was plotted against the cumulative time, a trend line and equation are added and the time at which the sample is fully saturated was obtained through interpolation. Figure 19 illustrates the process for each sample. For samples that were quickly saturated (CRB1, MFS1, and MFS2), a polynomial trend line was not the best option. In this case, a linear interpolation was carried out as it was considered the best solution. For samples

CS1, CS2, CS3, CLC1 and CRB2 full saturation was reached at the very first step, the time needed for saturation must be considered an overestimation for these samples.
The water saturation, wet weight, and time for each sample as well as the interpolated value for saturation time are reported in table 7.

Now the water saturation against time can be plotted for this case. All samples are present in the plot except for the coarse sandstone samples of which the saturation time was too short to observe any evolution. In fact, coarse sandstone samples seemed to have already saturated after only one or two seconds under pressure, which would raise the speculation that perhaps the samples were already saturated after the vacuum was broken and so, even before pressure was applied.
It is noticeable that in Figure 19, the lower permeability samples such as CRB3, CLC2 and CLC3 are easier to observe in terms of saturation evolution, while for the higher permeability samples, the evolution could not be captured graphically since they were saturated quickly and did not need so many steps.
It is worth pointing out that, after a few saturation attempts, some sediments were observed at the bottom of the water-filled container holding the sample at the end of the saturation process. Therefore, some samples were subject to grain loss during the saturation which may lead to an overestimation of porosity calculated with liquid saturation if not taken into consideration.

Table 6: Samples Saturation Porosity

Sample ID	*Dry Weight (g)*	*Wet Weight (g)*	*Bulk Volume (cc)*	*Porosity*
CS1	154.64	176.48	82.61	26.21%
CS2	155.186	176.46	82.17	25.67%
CS3	148.28	168.75	81.08	25.03%
CLC1	190.656	201.34	79.54	13.28%
CLC2	199.03	206.97	79.67	9.88%
CLC3	201.67	211.71	82.28	12.09%
CRB1	162.96	179.0	78.18	20.33%
CRB2	180.75	193.47	79.96	15.77%
CRB3	210.28	211.45	79.27	1.46%
MFS1	173.93	187.68	80.28	16.97%
MFS2	176.82	192.67	83.81	18.71%

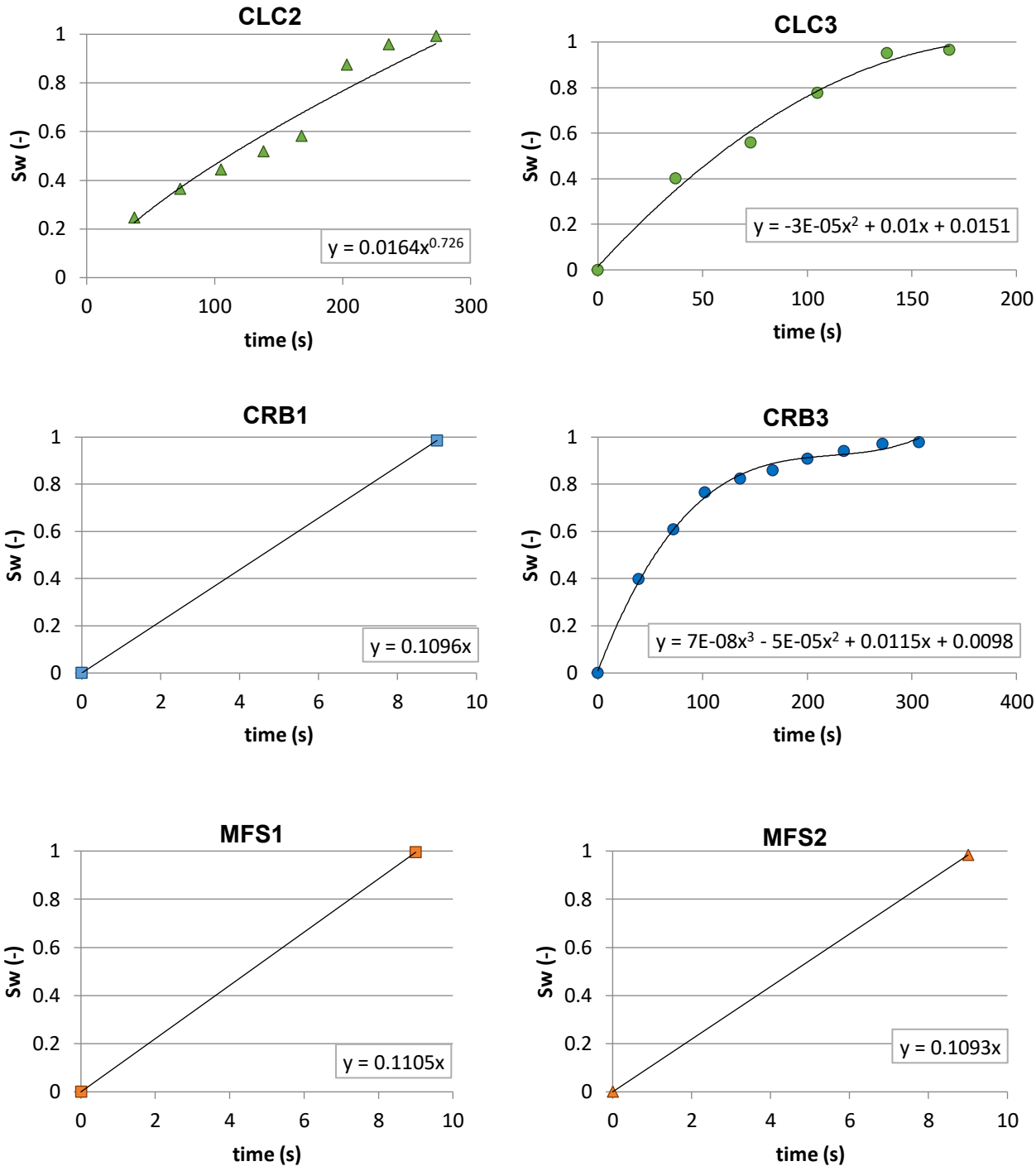

Figure 19: Saturation time interpolation (P = 800 psi)

Table 7: Samples Saturation at P=800psi

Sample ID	*Wet Weight (g)*	*Time (s)*	*Sw (-)*
CS1	154.64	0	0
	175.94	1	0.975
	176.48	2	1
CS2	155.19	0	0
	176.46	1	1
CS3	148.28	0	0
	168.75	1	1
CLC1	190.66	0	0
	201.31	5	1
	201.32	11	1.00075
CLC2	199.03	0	0
	201	37	0,247
	201.93	73	0.365
	202.57	105	0.445
	203.15	138	0.519
	203.66	168	0.583
	205.99	203	0.876
	206.64	236	0.958
	206.93	273	0.994
	206.97	312	1
interpolated		288	1
CLC3	201.68	0	0
	205.7	37	0.401
	207.28	73	0.558
	209.47	105	0.777
	211.23	138	0.952
	211.38	168	0.967
	211.71	203	1
interpolated		170	1
CRB1	162.96	0	0
	178.76	9	0.986
	178.99	17	1
	179.0	31	1.00093
interpolated		9	1
CRB2	180.75	0	0
	193.47	5	1
CRB3	210.28	0	0
	21075	39	0.399
	210.99	72	0.609
	211.18	102	0.766
	211.25	136	0.825
	211.29	167	0.861
	211.34	200	0.909

	211.38	235	0.941
	211.42	272	0.972
	211.43	307	0.979
	211.45	343	1
interpolated		315	1
MFS1	173.93	0	0
	187.6	9	0.995
	187.67	17	1
	187.68	31	1.00073
interpolated		9	1
MFS2	176.82	0	0
	192.37	9	0.983
	192.63	17	1
	192.64	31	1.00089
interpolated		31	1

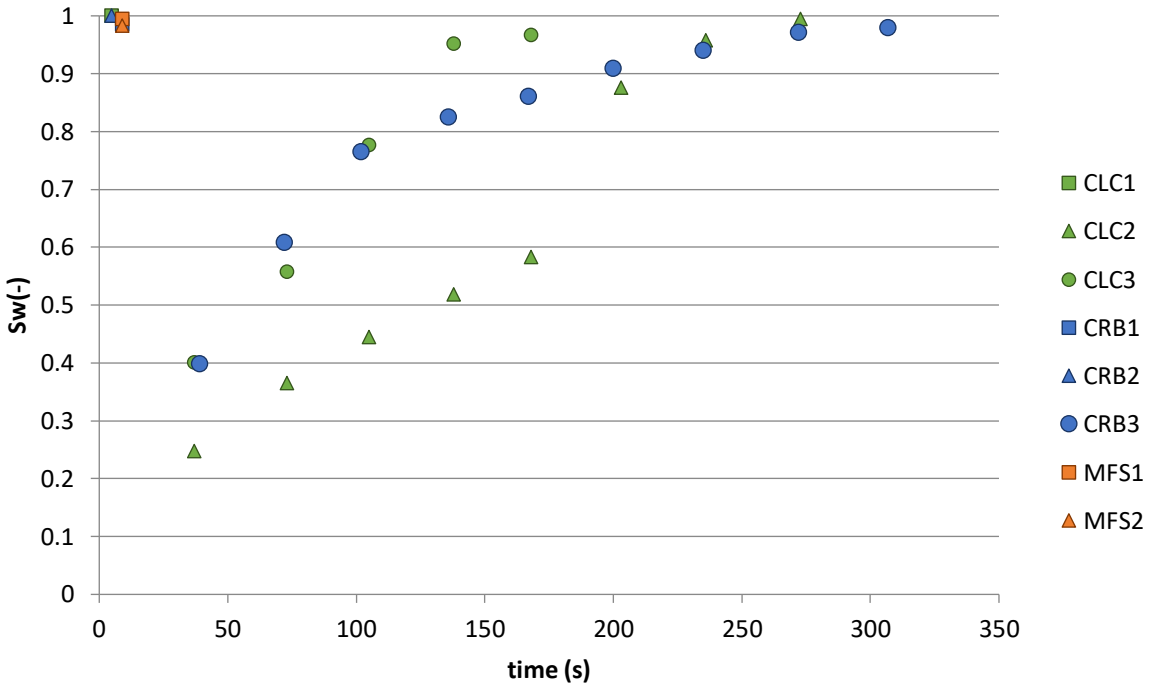

Figure 20: Evolution of Water Saturation at P=800psi

Table 8: Summary of Saturation at P=800psi

Sample ID	*Saturation Time (s)*	*Pressure Range (psi)*
CS1	2	800
CS2	1	800
CS3	1	800
CLC1	5	800
CLC2	288	700-800

CLC3	170	700-800
CRB1	9	800-900
CRB2	5	800
CRB3	315	780-800
MFS1	9	800-900
MFS2	9	800-900

4.3.3.2. Saturation at 1550 psi:

The saturation process was repeated for samples CLC2, CLC3 and CRB3 but the pressure was almost doubled this time. The test was expected to yield a lower saturation time, and therefore it was not performed for the rest of the samples which were saturated in a considerably brief time even in the 800 psi case.

The same methodology used before was followed, with the difference of setting the pressure of the chamber to around 1550 psi. Once again, the chamber was pressurized, and the samples were left to saturate. Pressure decreased slightly and it was more evident in this case than in the 800 psi case. It may also be attributed to pore space filling. Pressure ranges are reported in Table 10.

Saturation steps were carried out until a constant weight was reached, the saturation porosity of each sample was recalculated for the three samples and the interpolation for saturation time determination was done, although, due to a technical issue, (the malfunctioning of the check valve of the saturator), the measurements could not be completed. Thus, the time to reach full saturation was extrapolated from trend fitting the available data before the experiment interruption. The saturation values are reported in table 9.

It is already clear that, when compared with the previous case, the saturation time of the samples shortened. Even if it did not exactly cut the saturation time in half, it seemed that the time needed to reach a full saturation at a pressure of 1550 psi is around forty percent less than at 800 psi for two out of the three samples. A larger number of samples would yield more conclusive results.

Furthermore, when comparing the weights of samples CLC2 and CLC3 in both cases, it is noticeable that the weight increases in the case of 1550 psi. This could either be attributed to a more efficient saturation under higher pressure, or to the fact that the elevated pressure caused some fracturing inside the samples which allowed the infiltration of more water and therefore obtaining a higher wet weight. This last hypothesis is also sustained by the fact that some fractures were observed on the surface of these samples after the experiment.

Table 9: Samples Saturation at P=1550psi

Sample ID	*Wet Weight (g)*	*Time (s)*	*Sw (-)*
CRB3	210.3	0	0
	210.69	13	0.340
	210.89	26	0.519
	211	38	0.611

	211.06	52	0.666
	211.10	64	0.702
	211.17	76	0.757
	211.22	89	0.803
	211.28	102	0.859
	211.32	115	0.8903
	211.33	128	0.899
	211.38	143	0.942
Extrapolated		188	1
CLC2	199.34	0	0
	202.47	13	0.363
	203.68	26	0.505
	204.5	38	0.6
	205.32	52	0.695
	206.25	64	0.803
	207.07	76	0.899
	207.70	89	0.973
	207.82	102	0.987
	207.87	115	0.992
	207.84	128	0.989
	207.94	143	1
Extrapolated		191	1
CLC3	201.34	0	0
	205.92	13	0.463
	207.6	26	0.627
	209.15	38	0.789
	210.6	52	0.932
	211.2	64	0.996
	211.24	76	1
Interpolated		67	1

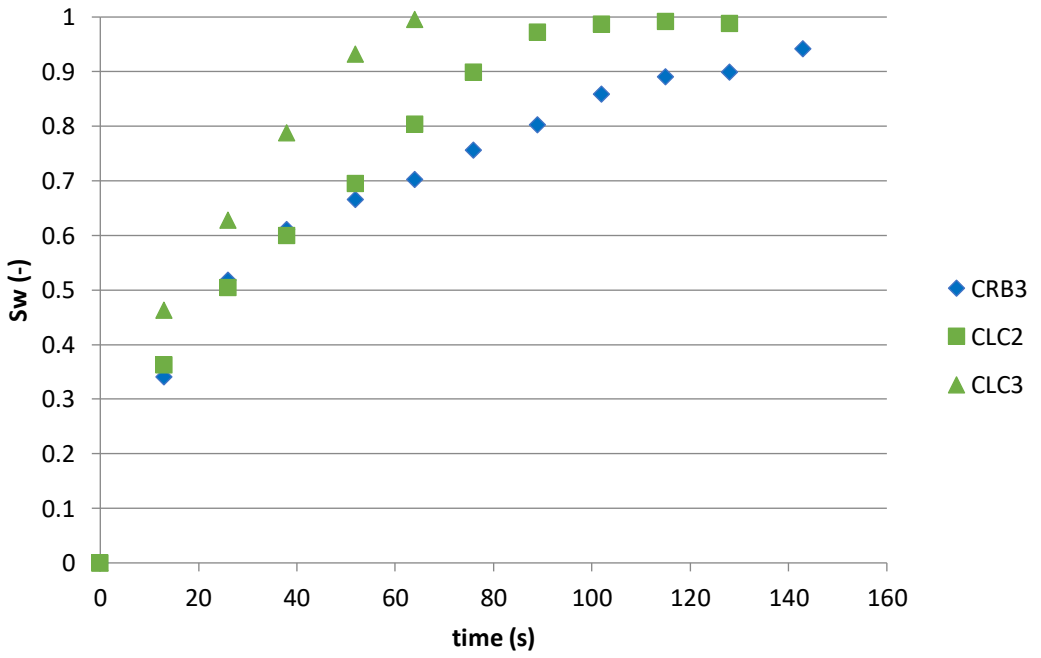

Figure 21: Evolution of Water Saturation at P=1550 psi

Table 10: Summary of Saturation at P=1550 psi

Sample ID	*Saturation Time (s)*	*Pressure Range (psi)*
CLC2	191	1500-1560
CLC3	67	1500-1560
CRB3	188	1500-1560

Chapter V: Discussion of Results:

In this chapter, the results obtained from experimentation will be analyzed in order to ultimately deduce appropriate conclusions.

5.1. Comparison of Porosity Data:

The porosity data obtained from the three methods employed (Grain Volume, Pore Volume, and Saturation Porosity) are subject to comparative analysis in order to assess the best method to measure the property.

In Figure 22, the difference in porosity data for each sample is represented. It is quite evident that the porosity obtained from grain volume (using the Matrix Cup) is generally higher than other porosity values, although the degree by which it differs varies depending on the rock type of the samples. For example, GV porosity seems to surpass both PV porosity and saturation porosity by a significant amount for coarse sandstones, meanwhile for carbonates the porosity values differ by 0.1 porosity units or less which is within experimental error ranges. [43]

Overall, if the porosity obtained from saturation is to be considered as the reference, it can be said that grain volume porosity measurement overestimates porosity for all samples except for calcarenites, while pore volume porosity measurements underestimate porosity values for coarse sandstones and calcarenites. Since PV porosities are missing for most of the carbonates and the medium-to-fine sandstones, a comparison cannot be made.

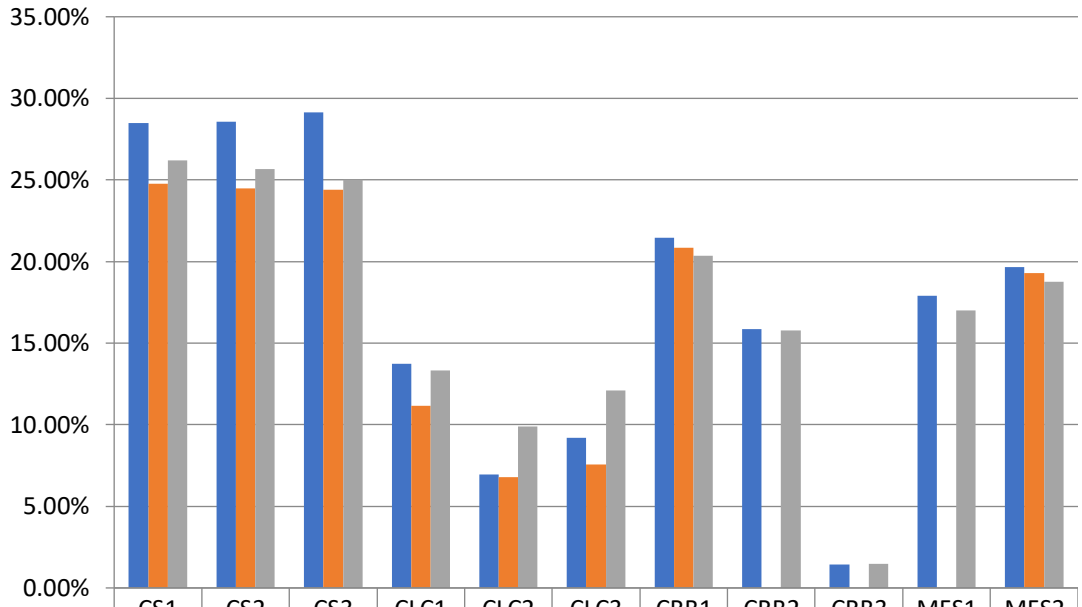

	CS1	CS2	CS3	CLC1	CLC2	CLC3	CRB1	CRB2	CRB3	MFS1	MFS2
Porosity GV	28.50%	28.58%	29.13%	13.75%	6.94%	9.21%	21.45%	15.86%	1.44%	17.92%	19.65%
Porosity PV	24.77%	24.49%	24.40%	11.15%	6.80%	7.58%	20.85%				19.31%
Saturation Porosity	26.21%	25.67%	25.03%	13.31%	9.88%	12.09%	20.34%	15.77%	1.46%	16.99%	18.75%

Figure 22: Comparison of Different Porosity Measurements

5.2. Saturation Time:

The petrophysical properties measured in this study are plotted with the saturation time in order to visualize any possible relationship between them.

5.2.1. Saturation time (800 psi) and absolute permeability:

In Figure 23, the time needed to reach 100% water saturation at 800 psi is plotted against the absolute permeability of each sample. Before the addition of any trend line, it looked like a certain trend may potentially fit the data. However, when trying to find a fitting trend, none seemed to be particularly appealing since none fitted all the points. In fact, the R^2 for a power function was around 71.3% even though the points seemed to be quite aligned. This led to questioning the presence of an outlier, which is not unheard of in experimental work. The first data to look at is the most unreliable. In this study, it is sample CLC2 for which, as explained in chapter IV, during permeability measurements the pressure drop was approaching the limit value above which non-Darcy behavior is observed. Moreover, the sample's Klinkenberg permeability was obtained using only three points due to the difficulty to measure gas permeability, while it is preferable to use at least four to five points to obtain a reliable permeability.

In Figure 24, the time needed to reach 100% water saturation of the samples at 800 psi was plotted against absolute permeability while removing the sample CLC2. A significant difference in the trend fitting the data is observed as the R^2 jumps to 99.3% without the presence of sample CLC2, which is an almost perfect power correlation between saturation time and absolute permeability. The power function becomes:

$$t_{sat} = 28.887 \cdot k_{abs}^{-0.466}$$

Equation 21

Where t_{sat} is the saturation time expressed in seconds (s) and k_{abs} is the absolute permeability of a rock sample.

Now that an empirical correlation was obtained between saturation time and absolute permeability, and having the saturation time for all the samples, an estimated value of permeability for sample CLC2 was found as well as for other samples for which the permeability was missing. The results are resumed in Table 11 and a new plot containing the extrapolated values of permeability is visualized in Figure 25.

The saturation time at 1550 psi was not plotted against absolute permeability, since only three samples were tested and only for two of them the extrapolated permeability value could be obtained.

Table 11: Extrapolated Values of Absolute Permeability

Sample ID	Extrapolated absolute permeability (mD)	Saturation time (s)
CLC2	0.00719	288
CRB2	43.1	5
CRB3	0.00593	315

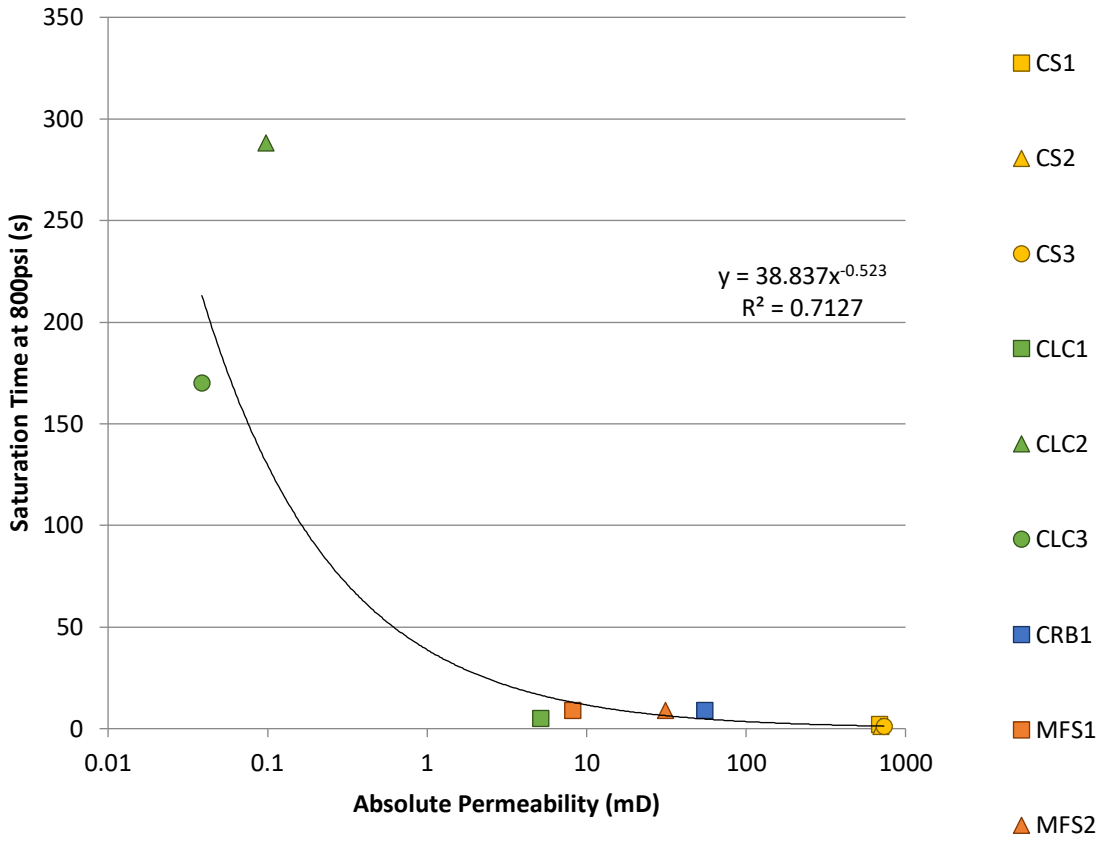

Figure 23: Saturation Time With Absolute Permeability

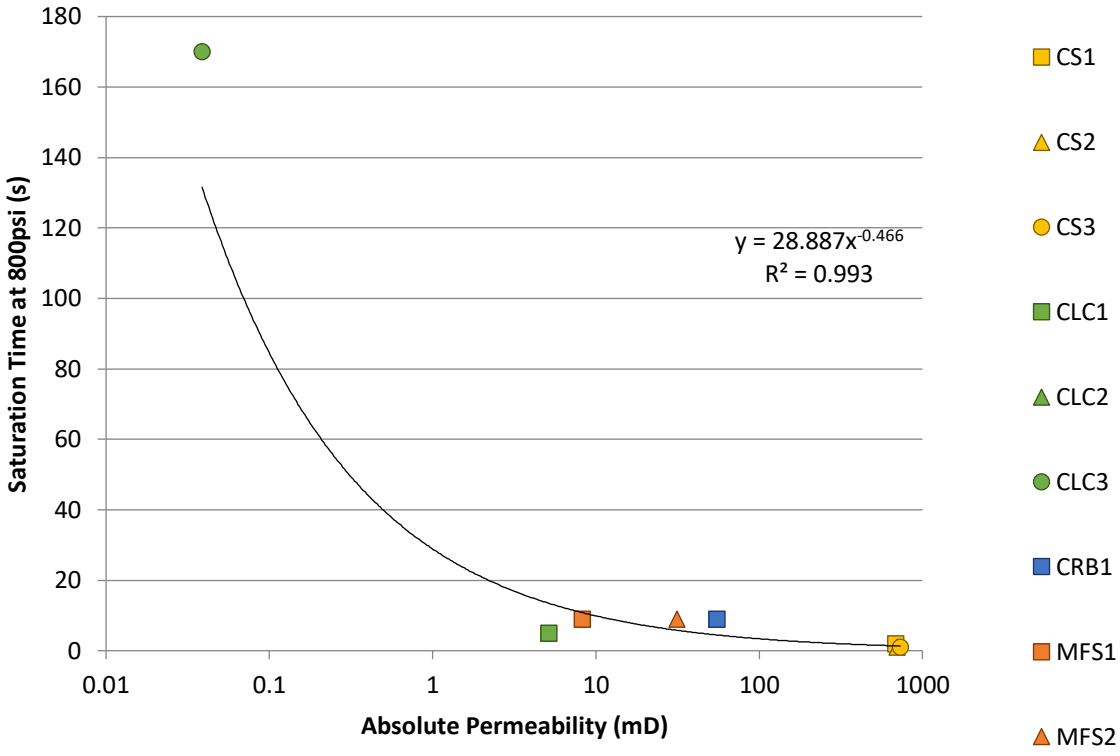

Figure 24: Saturation Time Against Absolute Permeability After Removing Sample CLC2

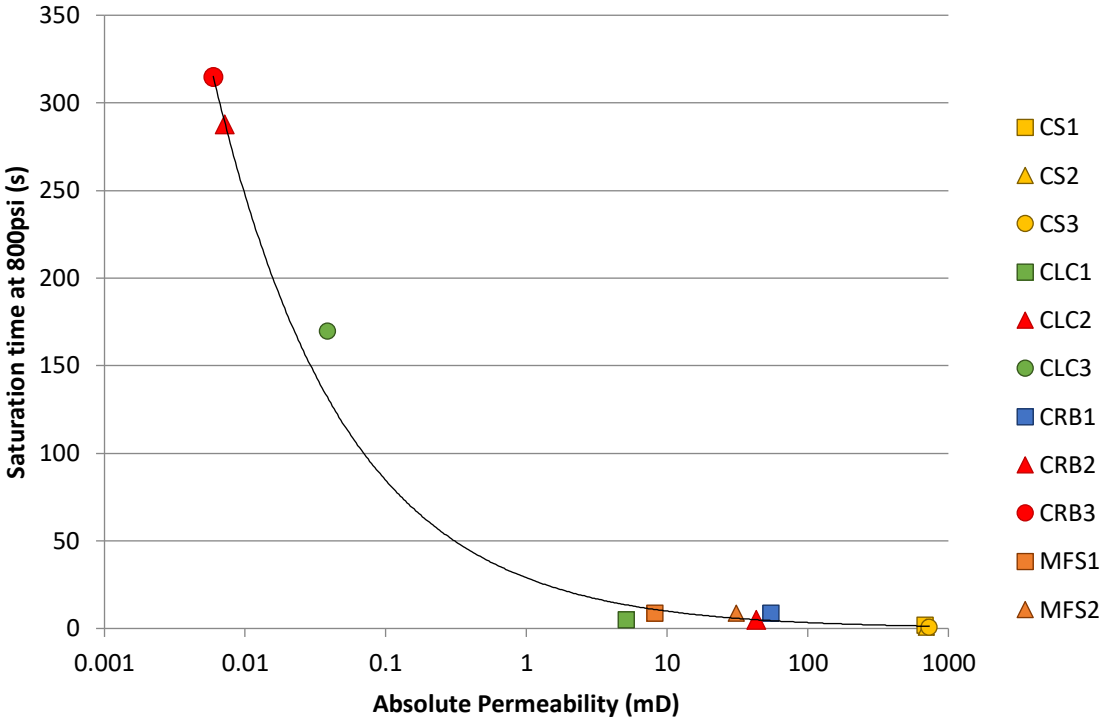

Figure 25: Saturation Time and Absolute Permeability with Extrapolated Permeabilities

5.2.2. Saturation time (800 psi) and porosity:

- **Saturation time and porosity:**

Table 12 contains the porosity estimated based on saturation, grain volume porosity (GV porosity), pore volume porosity (PV porosity) and 100% water saturation time of each sample. Although saturation time and permeability looked to have a nice trend even before trying to find a fitting function, it was not the case at first glance for saturation time plotted against the saturation porosity in Figure 26. The correlation between the two parameters in this case was around 54% for an exponential trend line which was found to be the best fit, and although in the previous case one point was considered unreliable while performing permeability measurements, there had been no problems with saturation porosity measurements. Therefore, all points should be considered.

When including graphs of other methods of porosity measurement (grain volume and pore volume) with saturation time (Figure 27), it was observed that sample CRB3 seems quite far from all the other points on the graph. Moreover, in the graph of PV porosity, the trend fit quite well without the presence of CRB3. To emphasize the difference this sample makes in the fitting, the plots were visualized again without sample CRB3 in Figure 28. A power correlation with R^2 higher than 90% was observed for all three plots, albeit the equations were not the same, which is logical considering that the values of porosity differ slightly between methods. The equations found are:

- For saturation porosity with an R^2 of 90.1%:

$$t_{sat} = 0.0014\Phi^{-5.003}$$

Equation 22

- For GV porosity with an R^2 of 94.7%:

$$t_{sat} = 0.0135\Phi^{-3,678}$$

Equation 23

- For PV porosity with R^2 of 97.7%:

$$t_{sat} = 0{,}0108\Phi^{-3,609}$$

Equation 24

The equations obtained for grain volume porosity (GV porosity) and pore volume porosity (PV porosity) are quite similar, but they differ from the equation estimated for saturation porosity. Having obtained a correlation for PV porosity, the missing PV porosity values can now be estimated using Equation 24.

The estimated PV porosities reported in Table 12 show inconsistent values with respect to the two other methods, especially for sample CRB3. It must be highlighted that for samples CRB2 and MFS1 the time needed to reach full water saturation might be overestimated, adding uncertainties in this PV porosity estimation process.

Finally, the saturation time at 1550 psi was not plotted against porosity since only three samples were tested, and two of them were probably fractured.

Table 12: Three Porosity Measurements and Saturation Time

Sample ID	*Saturation Porosity*	*Porosity GV*	*Porosity PV*	*100% Water Saturation time (s)*
CS1	26.21%	28.50%	24.77%	2
CS2	25.67%	28.58%	24.49%	1
CS3	25.03%	29.13%	24.40%	1
CLC1	13.28%	13.75%	11.15%	5
CLC2	9.88%	6.94%	6.80%	288
CLC3	12.09%	9.21%	7.58%	170
CRB1	20.33%	21.45%	20.85%	9
CRB2	15.77%	15.86%	18.26%*	5
CRB3	1.46%	1.44%	5.79%*	315
MFS1	16.97%	17.92%	15.51%*	9
MFS2	18.71%	19.65%	19.31%	9

*Estimated using Equation 24

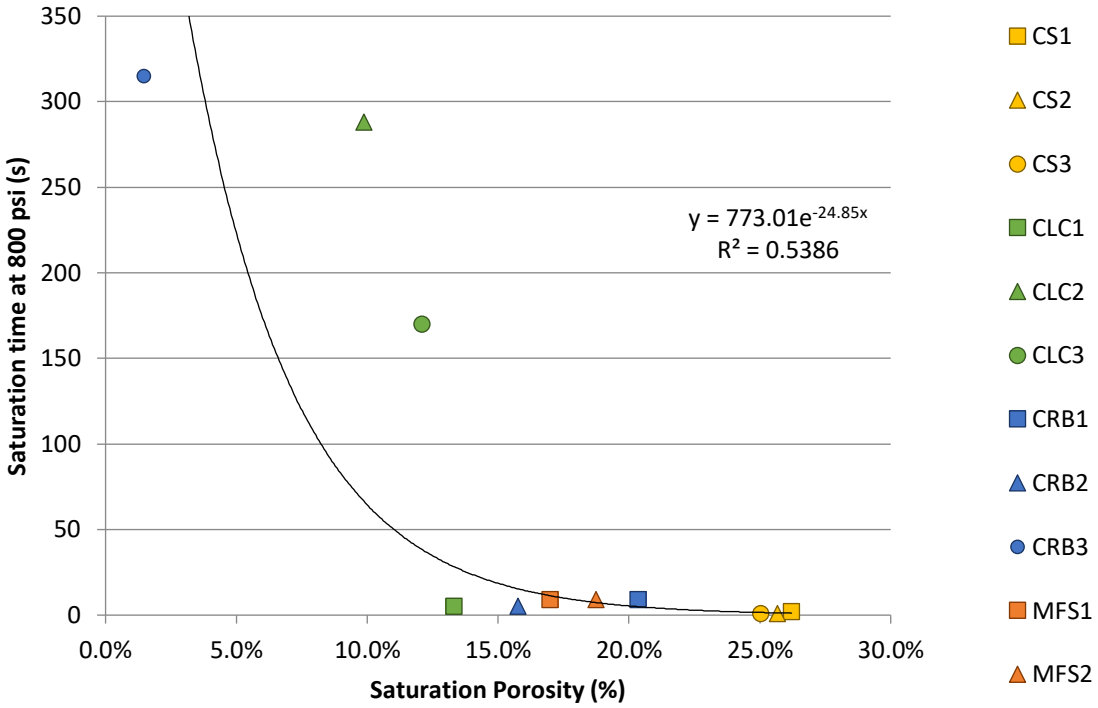

Figure 26: Saturation Time against Saturation Porosity

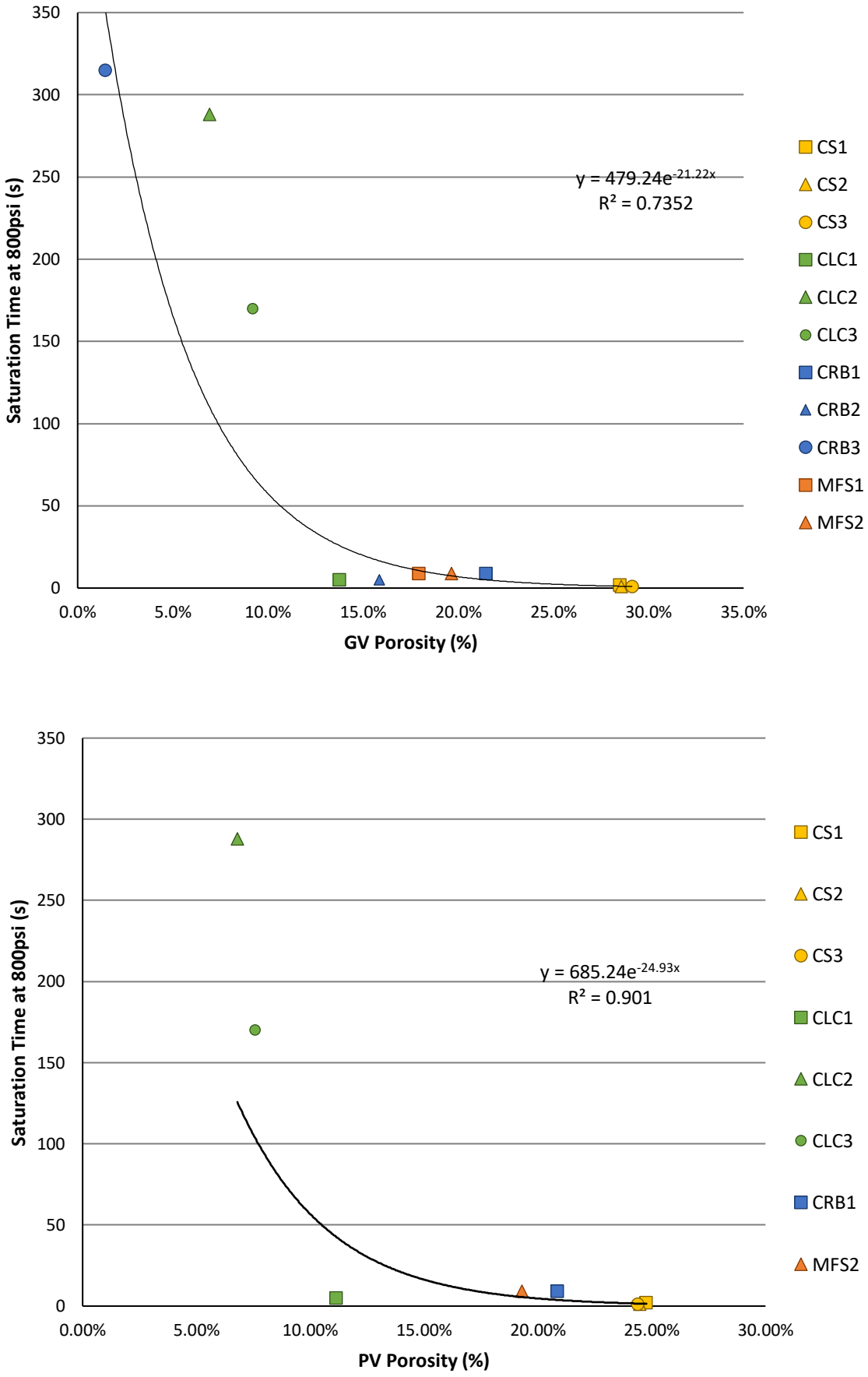

Figure 27: Saturation Time against GV Porosity (Top) and against PV Porosity (Bottom)

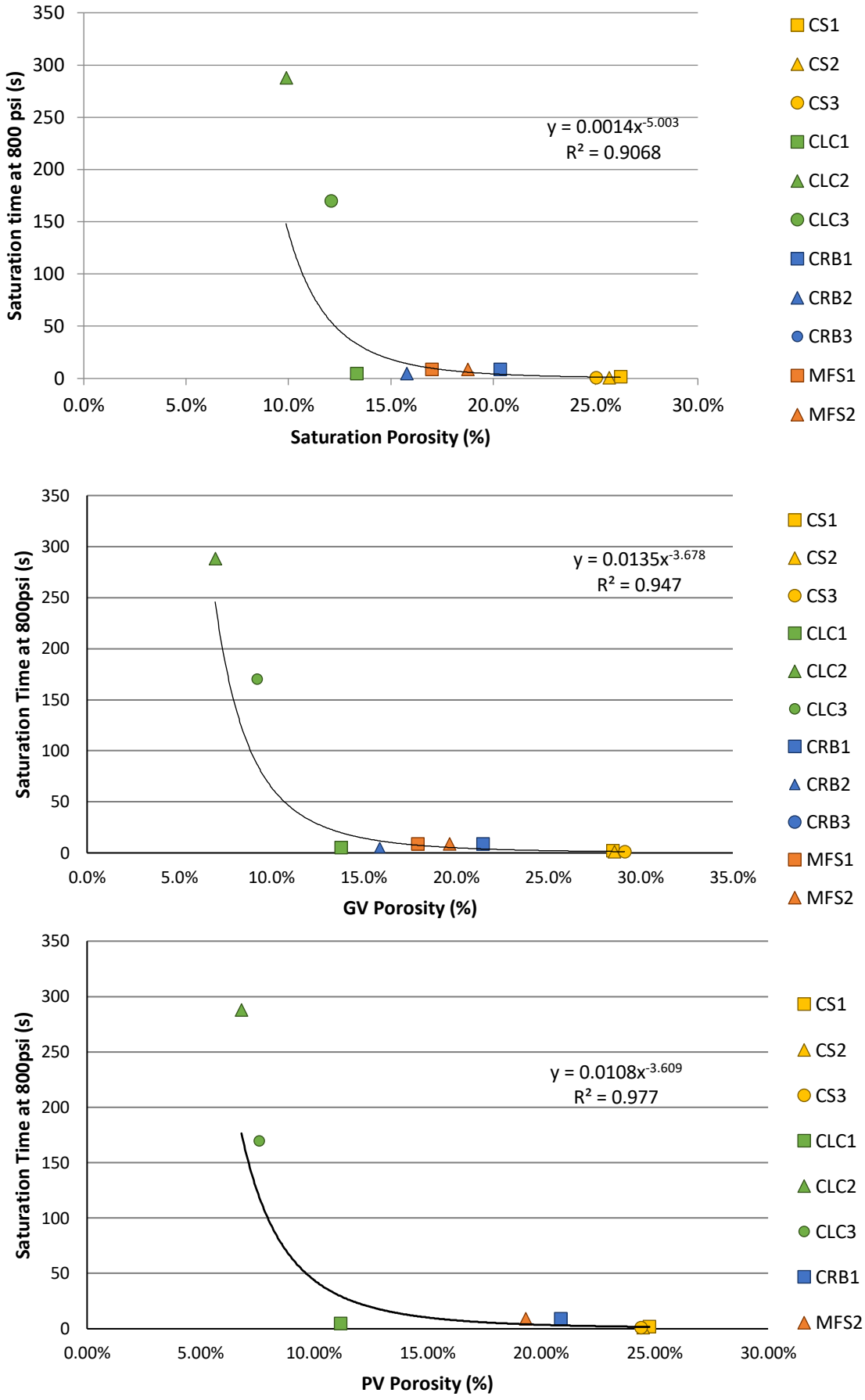

Figure 28: Saturation time against Saturation Porosity (Top), GV Porosity (Middle) and PV Porosity (Bottom) after removal of CRB3

5.3. Analysis by Rock Type

When categorizing the samples by rock type, it is noticeable in Table 13 that similar ranges of saturation porosity and saturation time were found for coarse and medium-to-fine sandstones, but this was not the case for calcarenites and carbonates, for which completely different results of saturation time were obtained even if the rock type was the same.
Furthermore, the permeability values in coarse sandstones do not differ much, while in medium-to-fine sandstones they vary in a significant way. For calcarenites, the permeability varies by two orders of magnitude from 0.0387 mD for CLC3 to 5.15 mD for CLC1 even if the samples are of the same rock type.
Eventually, within carbonates porosity seemed to differ a lot, from 1.46% for CRB3, to 15.77% and 20.33% for CRB2 and CRB1, respectively.

Table 13: Saturation Porosity, Absolute Permeability (With Extrapolated Values) and Saturation Time

Sample ID	Saturation Porosity	Permeability kL (mD)	Saturation time (s)
CS1	26.21%	686	2
CS2	25.67%	700	1
CS3	25.03%	731.5	1
CLC1	13.28%	5.15	5
CLC2	9.88%	0.0977*	288
CLC3	12.09%	0.0387	170
CRB1	20.33%	55.2	9
CRB2	15.77%	43.1*	5
CRB3	1.46%	0.00593*	315
MFS1	16.97%	8.21	9
MFS2	18.71%	31.23	9

*Extrapolated using Equation 21

Chapter VI: Conclusion:

In this study, the rock dimensions, and the dry weight of 11 different samples were measured. After that, their petrophysical properties were measured, namely porosity and permeability. First, porosity was assessed using two different methods (grain volume and pore volume), then absolute permeability to gas was measured and corrected to absolute permeability to liquids using the Klinkenberg correlation. The sample absolute permeability to liquid ranges between 0.04 mD and 732 mD, while their porosities are in the range of 1.4-29.1%. Then, the samples were subject to multiple saturation experiments: the first saturation process was performed at atmospheric pressure. The samples were then dried, and another saturation procedure was applied using a manual saturator at a pressure of 800 psi until the wet weight of each sample became constant. The wet and dry weights of each sample were exploited to calculate water saturation at each time step. The evolution of water saturation with time was plotted until 100% water saturation was reached. Finally, the samples which were slowest to saturate were dried again, and the saturation process was repeated with a pressure of 1550 psi. This final set of experiments was not completed due to technical issues, but the amount of data collected was enough to obtain consistent results.

After arranging and analyzing the experimental data, the following conclusions can be made:

- Atmospheric pressure is not enough to fully saturate any of the available samples even if they were left to saturate for a dozen days. In fact, the highest recorded water saturation (based on porosity calculated through pore volume) at atmospheric pressure was 88.3% for coarse sandstone sample CS3. Coarse sandstones were expected to be fully saturated even at atmospheric pressure due to their high permeability, but it came as a surprise that not even one sample of the available set was fully saturated. Nevertheless, among the samples that were subject to saturation at atmospheric pressure, coarse sandstones resulted in the highest saturations even if they did not reach 100%. Perhaps a study could be conducted where sandstone samples are left to saturate for longer periods to be able to conclude with certainty that 100% water saturation cannot be reached regardless of the time the samples are soaked. No information on this matter was found in the literature as well as no experiments of this kind had been conducted to confirm whether this is always true. When the samples are put under pressure, 100% saturation is reachable. Moreover, saturations theoretically estimated based on the porosity measured with the core holder (Pore Volume) were exceeding 100%: this occurrence was the same which led to the conclusion that samples were not saturated after immersion in water at atmospheric pressure.
- When comparing saturation processes under different pressures, it appears that the saturation time is shortened when higher pressures are applied but not necessarily by the same proportion as the pressure increase. In this study, the pressure almost doubled from 800 psi to 1550 psi, but the time needed to fully saturate the samples was not cut by half. For example, the time needed to fully saturate sample CRB3 was reduced from 315 seconds (about 5 and a half minutes) at 800 psi to 188 seconds

(about 3 minutes) at 1550 psi, which is around a 40% reduction of the saturation time. Furthermore, at 1550 psi, some fractures were spotted on two calcarenites (CLC2 and CLC3), and the wet weight when fully saturated was higher at 1550 psi than for the case of 800 psi which may be interpreted as the water filling the fractures besides the pores. In fact, the highest registered wet weight for sample CLC2 at 800 psi was 206.97 g, while it reached 207.94 g in the case of 1550 psi. Three samples are not enough to conclusively establish a relationship between the saturation time and pressure, thus a larger set of samples of various properties should be used for any further work.

- When the time needed to read 100% water saturation was plotted against absolute permeability, a power correlation was potentially found. The function obtained from the experimental data is:

$$t_{sat} = 28.887 \cdot k_{abs}^{-0.466}$$

Equation 25

This empirical correlation was obtained after removing one point from the plot (sample CLC2) as it was considered an outlier. In fact, the permeability for this sample was obtained with a high degree of uncertainty starting from the unreliability of the gas permeability measurements as they approached non-Darcy behavior. In fact, a permeability lower than its current 0.1 mD was expected for sample CLC2 since it was slower to saturate if compared to sample CLC3, which instead has a permeability of 0.0387 mD. By assuming the obtained saturation time function as true, a corrected permeability of 0.00719 mD was estimated for sample CLC2. Furthermore, the correlation was also used to estimate the missing permeabilities of samples CRB2 and CRB3.

In order for this correlation to be validated, a lot more samples need to be tested with a wide range of different petrophysical properties. In fact, it would be recommended in the future to test samples with lower permeabilities since the curve obtained in this study relies on very few points below 5 mD.

- When the time to fully saturate the samples was plotted against porosity calculated using wet and dry weights of each sample or GV porosity, no significant correlation was found at first. But, when one sample that was quite isolated on the graph was removed, a power correlation with an R^2 of more than 90% was observed for the time to reach 100% saturation versus porosity (saturation porosity, GV porosity and PV porosity). Even if a potential correlation was found between porosity and saturation time, testing a larger number of samples is needed in order to confirm this possible relationship.
- When categorizing samples by rock type, differences in the petrophysical properties can be observed within samples of the same rock type. In fact, in the set of carbonates used in this study, porosity varies from 1.46% for CRB3 to 20.33% for CRB1, which represents a huge variation. Another evidence can be found for the permeability of

calcarenites which varies from micro-Darcy for CLC2 and CLC3, if its value of permeability estimated using the correlation is to be considered as correct, to 5.15 mD for CLC1.

Some issues were encountered during the experiments. The first one was that the samples were gaining some weight after drying and leaving them overnight; this was attributed to ambient humidity. To avoid this, one recommendation may be to store the samples in a dehumidified and closed container. Another issue faced was grain loss and deposition of sediments at the bottom of the tank in the saturator. This brings the problem of inaccuracies when measuring the wet weight. A recommendation may be to try to make sure the sample is well consolidated before any test and always report the observation of grain loss. It is also suggested to measure the weight of the sample prior to each experiment. This issue also represents a potential problem of clogging due to particle deposition in the wet circuit of the equipment. Actually, clogging inside the check valves was the reason for the failure of a part of the experiments. The implementation of a filter between the chamber in which the samples are saturated and the rest of the water circuit may be a good solution. The final issue was the fracturing of samples CLC2 and CLC3 when saturated at 1550 psi. It is important to make sure that the saturating pressure is not too high or not increased too sharply in order not to damage the samples, especially when they seem brittle at first look.

Bibliography:

[1]
D. Tiab and E. C. Donaldson, “Reservoir Characterization,” in Petrophysics, Elsevier, 2016, pp. 583–640. doi: 10.1016/B978-0-12-803188-9.00010-3.
[2]
F. Aminzadeh, Ed., Reservoir characterization: fundamentals and applications. in Sustainable Energy Engineering, no. 2. Beverly, Mass: Srivener Publishing, 2022.
[3]
“Reservoir Characterization and Modeling: A Look Back to See the Way Forward,” in Uncertainty Analysis and Reservoir Modeling, American Association of Petroleum Geologists, 2011, pp. 289–309. doi: 10.1306/13301421M963458.
[4]
F. Aminzadeh and S. N. Dasgupta, Geophysics for petroleum engineers, First edition. in Developments in petroleum science, no. volume 60. Amsterdam; Boston: Elsevier, 2013.
[5]
R. O. Baker, H. W. Yarranton, and J. L. Jensen, “Reservoir Characterization Methods,” in Practical Reservoir Engineering and Characterization, Elsevier, 2015, pp. 349–434. doi: 10.1016/B978-0-12-801811-8.00010-9.
[6]
D. Patrick Murphy, G. V. Chilingarian, and S. Jalal Torabzadeh, “Chapter 3 Core analysis and its application in reservoir characterization,” in Developments in Petroleum Science, Elsevier, 1996, pp. 105–153. doi: 10.1016/S0376-7361(96)80025-2.
[7]
V. Tavakoli, Geological Core Analysis. in SpringerBriefs in Petroleum Geoscience & Engineering. Cham: Springer International Publishing, 2018. doi: 10.1007/978-3-319-78027-6.
[8]
R. M. Holt, E. Fjaer, O. Torsaeter, and S. Bakke, “Petrophysical laboratory measurements for basin and reservoir evaluation,” Marine and Petroleum Geology, vol. 13, no. 4, pp. 383–391, Jun. 1996, doi: 10.1016/0264-8172(95)00091-7.
[9]
C. McPhee, J. Reed, and I. Zubizarreta, Core analysis: a best practice guide, First edition. in Developments in petroleum science, no. volume 64. Amsterdam Boston, Mass. Heidelberg [und 9 andere]: Elsevier, 2015.
[10]
M. Bashiri, M. Kamari, and G. Zargar, “An Improvement in Cation Exchange Capacity Estimation and Water Saturation Calculation in Shaly Layers for One of Iranian Oil Fields,” IJOGST, vol. 6, no. 1, Jan. 2017, doi: 10.22050/ijogst.2017.44376.
[11]
S. Borazjani et al., “Determining water-oil relative permeability and capillary pressure from steady-state coreflood tests,” Journal of Petroleum Science and Engineering, vol. 205, p. 108810, Oct. 2021, doi: 10.1016/j.petrol.2021.108810.
[12]
N. Hemmati et al., “Laboratory validation of steady-state-transient test to determine relative permeability and capillary pressure,” Fuel, vol. 321, p. 123940, Aug. 2022, doi: 10.1016/j.fuel.2022.123940.
[13]

E. Sripal, D. Grant, and L. James, “Application of SEM Imaging and MLA Mapping Method as a Tool for Wettability Restoration in Reservoir Core Samples for SCAL Experiments,” Minerals, vol. 11, no. 3, p. 285, Mar. 2021, doi: 10.3390/min11030285.
[14]
E. Heydari-Farsani, J. E. Neilson, G. I. Alsop, and H. Hamidi, “The effect of rock type on natural water flooding and residual oil saturation below free water level and oil water contact: A case study from the Middle East,” Journal of Petroleum Science and Engineering, vol. 193, p. 107392, Oct. 2020, doi: 10.1016/j.petrol.2020.107392.
[15]
M. Shabani, S. Yarmohammadi, and S. Ghaffary, “Reservoir quality investigation by combination of core measured data and NMR technique analysis: a case study of Asmari carbonate reservoir in Gachsaran field,” Carbonates Evaporites, vol. 38, no. 1, p. 1, Mar. 2023, doi: 10.1007/s13146-022-00824-y.
[16]
E. Lock, M. Ghasemi, M. Mostofi, and V. Rasouli, “An experimental study of permeability determination in the lab,” Koya, University, Kurdistan, Dec. 2012, pp. 221–230. doi: 10.2495/PMR120201.
[17]
B. S. Nabawy and M. Kh. Barakat, “Formation evaluation using conventional and special core analyses: Belayim Formation as a case study, Gulf of Suez, Egypt,” Arab J Geosci, vol. 10, no. 2, p. 25, Jan. 2017, doi: 10.1007/s12517-016-2796-9.
[18]
M. Jamshidian, M. Mansouri Zadeh, M. Hadian, R. Moghadasi, and O. Mohammadzadeh, “A novel estimation method for capillary pressure curves based on routine core analysis data using artificial neural networks optimized by Cuckoo algorithm – A case study,” Fuel, vol. 220, pp. 363–378, May 2018, doi: 10.1016/j.fuel.2018.01.099.
[19]
F. Civan, “Petrophysical Alterations—Fluid Disposition, Distribution, and Entrapment, Flow Functions, and Petrophysical Parameters of Geologic Formations,” in Reservoir Formation Damage, Elsevier, 2016, pp. 127–166. doi: 10.1016/B978-0-12-801898-9.00006-0.
[20]
C. Delle Piane and J. Sarout, “Effects of water and supercritical CO2 on the mechanical and elastic properties of Berea sandstone,” International Journal of Greenhouse Gas Control, vol. 55, pp. 209–220, Dec. 2016, doi: 10.1016/j.ijggc.2016.06.001.
[21]
T. Ahmed, “Fundamentals of Rock Properties,” in Reservoir Engineering Handbook, Elsevier, 2010, pp. 189–287. doi: 10.1016/B978-1-85617-803-7.50012-2.
[22]
T. A.-A. O. Ganat, “Porosity,” in Fundamentals of Reservoir Rock Properties, Cham: Springer International Publishing, 2020, pp. 5–24. doi: 10.1007/978-3-030-28140-3_2.
[23]
D. Tiab and E. C. Donaldson, “Porosity and Permeability,” in Petrophysics, Elsevier, 2016, pp. 67–186. doi: 10.1016/B978-0-12-803188-9.00003-6.
[24]
J.-Q. Shi, Z. Xue, and S. Durucan, “Supercritical CO2 core flooding and imbibition in Berea sandstone — CT imaging and numerical simulation,” Energy Procedia, vol. 4, pp. 5001–5008, 2011, doi: 10.1016/j.egypro.2011.02.471.
[25]

J.-Q. Shi, Z. Xue, and S. Durucan, “Supercritical CO2 core flooding and imbibition in Tako sandstone—Influence of sub-core scale heterogeneity,” International Journal of Greenhouse Gas Control, vol. 5, no. 1, pp. 75–87, Jan. 2011, doi: 10.1016/j.ijggc.2010.07.003.
[26]
L. Zhang, “Permeability,” in Engineering Properties of Rocks, Elsevier, 2017, pp. 339–370. doi: 10.1016/B978-0-12-802833-9.00008-0.
[27]
R. Wheaton, “Basic Rock and Fluid Properties,” in Fundamentals of Applied Reservoir Engineering, Elsevier, 2016, pp. 5–57. doi: 10.1016/B978-0-08-101019-8.00002-8.
[28]
L. Klinkenberg, “The Permeability of Porous Media To Liquids and Gases,” in The Permeability of Porous Media To Liquids and Gases, API-41-200.in Drilling and Production Practice. New York: API-41-200, 1941.
[29]
C. McPhee, J. Reed, and I. Zubizarreta, “Capillary Pressure,” in Developments in Petroleum Science, Elsevier, 2015, pp. 449–517. doi: 10.1016/B978-0-444-63533-4.00009-3.
[30]
E. C. Donaldson and W. Alam, Wettability. Houston, Tex: Gulf Pub. Co, 2008.
[31]
S. Peng, “Advanced understanding of gas flow and the Klinkenberg effect in nanoporous rocks,” Journal of Petroleum Science and Engineering, vol. 206, p. 109047, Nov. 2021, doi: 10.1016/j.petrol.2021.109047.
[32]
B. L. Alemu, E. Aker, M. Soldal, Ø. Johnsen, and P. Aagaard, “Effect of sub-core scale heterogeneities on acoustic and electrical properties of a reservoir rock: a CO_2 flooding experiment of brine saturated sandstone in a computed tomography scanner: Effect of sub-core scale heterogeneities on a reservoir rock,” Geophysical Prospecting, vol. 61, no. 1, pp. 235–250, Jan. 2013, doi: 10.1111/j.1365-2478.2012.01061.x.
[33]
F. Trippetta, R. Ruggieri, M. Brandano, and C. Giorgetti, “Petrophysical properties of heavy oil-bearing carbonate rocks and their implications on petroleum system evolution: Insights from the Majella Massif,” Marine and Petroleum Geology, vol. 111, pp. 350–362, Jan. 2020, doi: 10.1016/j.marpetgeo.2019.08.035.
[34]
J. S. Gomes, M. T. Ribeiro, C. J. Strohmenger, S. Negahban, and M. Z. Kalam, “Carbonate Reservoir Rock Typing – The Link between Geology and SCAL,” Abu Dhabi, UAE: SPE, Nov. 2008, p. SPE-118284-MS. doi: 10.2118/118284-MS.
[35]
M. Barbier, M. Floquet, Y. Hamon, and J.-P. Callot, “Nature and distribution of diagenetic phases and petrophysical properties of carbonates: The Mississippian Madison Formation (Bighorn Basin, Wyoming, USA),” Marine and Petroleum Geology, vol. 67, pp. 230–248, Nov. 2015, doi: 10.1016/j.marpetgeo.2015.05.026.
[36]
S. Akin, J. M. Schembre, S. K. Bhat, and A. R. Kovscek, “Spontaneous imbibition characteristics of diatomite,” Journal of Petroleum Science and Engineering, vol. 25, no. 3–4, pp. 149–165, Mar. 2000, doi: 10.1016/S0920-4105(00)00010-3.
[37]
Q. Hu et al., “Petrophysical properties of representative geological rocks encountered in carbon storage and utilization,” Energy Reports, vol. 9, pp. 3661–3682, Dec. 2023, doi: 10.1016/j.egyr.2023.02.020.

[38]
Á. Rabat, R. Tomás, and M. Cano, “Advances in the understanding of the role of degree of saturation and water distribution in mechanical behaviour of calcarenites using magnetic resonance imaging technique,” Construction and Building Materials, vol. 303, p. 124420, Oct. 2021, doi: 10.1016/j.conbuildmat.2021.124420.
[39]
S. Zakeri, R. Hazlett, and K. Babu, “An analytic solution for Counter-Current spontaneous imbibition in porous media by the perturbation method,” Journal of Hydrology, vol. 618, p. 129181, Mar. 2023, doi: 10.1016/j.jhydrol.2023.129181.
[40]
D. Wang, X. Bian, H. Qin, D. Sun, and B. Yu, “Experimental Investigation of Mechanical Properties and Failure Behavior of Fluid-Saturated Hot Dry Rocks,” Nat Resour Res, vol. 30, no. 1, pp. 289–305, Feb. 2021, doi: 10.1007/s11053-020-09760-x.
[41]
C. Pichler, R. Lackner, T. Bader, and L. Perfler, “Water vapor diffusion properties of Obernkirchener sandstone: Analysis of DVS data,” Construction and Building Materials, vol. 347, p. 128554, Sep. 2022, doi: 10.1016/j.conbuildmat.2022.128554.
[42]
C. Franzen and P. W. Mirwald, “Moisture content of natural stone: static and dynamic equilibrium with atmospheric humidity,” Env Geol, vol. 46, no. 3–4, Aug. 2004, doi: 10.1007/s00254-004-1040-1.
[43]
D. L. Luffel and W. E. Howard, “Reliability of Laboratory Measurement of Porosity in Tight Gas Sands,” SPE Formation Evaluation, vol. 3, no. 04, pp. 705–710, Dec. 1988, doi: 10.2118/16401-PA.
[44]
D. Tiab and E. C. Donaldson, “Formation Resistivity and Water Saturation,” in Petrophysics, Elsevier, 2016, pp. 187–278. doi: 10.1016/B978-0-12-803188-9.00004-8.
[45]
W. Tanikawa and T. Shimamoto, “Klinkenberg effect for gas permeability and its comparison to water permeability for porous sedimentary rocks,” Jul. 2006. doi: 10.5194/hessd-3-1315-2006.
[46]
U. Kuila, D. K. McCarty, A. Derkowski, T. B. Fischer, and M. Prasad, “Total porosity measurement in gas shales by the water immersion porosimetry (WIP) method,” Fuel, vol. 117, pp. 1115–1129, Jan. 2014, doi: 10.1016/j.fuel.2013.09.073.
[47]
F. Marica, Q. Chen, A. Hamilton, C. Hall, T. Al, and B. J. Balcom, “Spatially resolved measurement of rock core porosity,” Journal of Magnetic Resonance, vol. 178, no. 1, pp. 136–141, Jan. 2006, doi: 10.1016/j.jmr.2005.09.003.
[48]
T. W. Melnyk and A. M. M. Skeet, “An improved technique for the determination of rock porosity,” Can. J. Earth Sci., vol. 23, no. 8, pp. 1068–1074, Aug. 1986, doi: 10.1139/e86-107.
[49]
R. P. Monicard, Properties of Reservoir Rocks: Core Analysis. Dordrecht: Springer Netherlands, 1980. doi: 10.1007/978-94-017-5016-5.